View metadata, citation and similar papers at core.ac.uk

brought to you by CORE

provided by ACMAC

ΠΑΝΕΠΙΣΤΗΜΙΟ ΚΡΗΤΗΣ - ΤΜΗΜΑ ΕΦΑΡΜΟΣΜΕΝΩΝ ΜΑΘΗΜΑΤΙΚΩΝ
Archimedes Center for Modeling, Analysis & Computation
UNIVERSITY OF CRETE - DEPARTMENT OF APPLIED MATHEMATICS
Archimedes Center for Modeling, Analysis & Computation

ACMAC's PrePrint Repository

Enhanced statistical stability in coherent interferometric imaging

Liliana Borcea and Josselin Garnier and George Papanicolaou and Chrysoula Tsogka

Original Citation:

Borcea, Liliana and Garnier, Josselin and Papanicolaou, George and Tsogka, Chrysoula

(2011)

Enhanced statistical stability in coherent interferometric imaging.

Inverse Problems, 27 (8). 085004. ISSN 0266-5611

This version is available at: http://preprints.acmac.uoc.gr/58/
Available in ACMAC's PrePrint Repository: February 2012

ACMAC's PrePrint Repository aim is to enable open access to the scholarly output of ACMAC.

http://preprints.acmac.uoc.gr/

ENHANCED STATISTICAL STABILITY IN COHERENT INTERFEROMETRIC IMAGING

LILIANA BORCEA*, JOSSELIN GARNIER†, GEORGE PAPANICOLAOU†, AND CHRYSOULA TSOGKA§

Abstract. We analyze the resolution and statistical fluctuations of images when the ambient medium is random and scattering can be modeled primarily by wavefront distortion. We compare the coherent interferometric imaging method to the widely used Kirchhoff migration and show how the latter loses statistical stability at an exponential rate with the distance of propagation. In Kirchhoff migration we form images by superposing the array data back propagated to the image domain. In coherent interferometry we back propagate local cross correlations of the array data. This is a denoising process that enhances the signal-to-noise ratio of images but also reduces the resolution. We quantify analytically the trade-off between enhanced stability and reduced resolution in coherent interferometric imaging.

Key words. array imaging, coherent interferometric imaging, data denoising, image resolution.

1. Introduction. We study the mathematical problem of imaging remote sources or reflectors in heterogeneous (cluttered) media with passive and active arrays of sensors. Because the inhomogeneities in the medium are not known, and they cannot be estimated in detail from the data gathered at the array, we model the uncertainty about the clutter with spatial random perturbations of the wave speed. The goal is to carry out analytically a comparative study of the resolution and signal-to-noise ratio (SNR) of two array imaging methods: the widely used Kirchhoff migration (KM) and coherent interferometry (CINT). By noise in the images we mean fluctuations that are due to the random medium.

Kirchhoff migration [5, 6] and its variants are widely used in seismic inversion, radar [14] and elsewhere. It forms images by superposing the wave fields received at the array, delayed by the travel times from the array sensors to the imaging points. KM works well in smooth and known media, where there is no wave scattering and the travel times can be estimated accurately. It also works well with data that has additive, uncorrelated measurement noise, provided the array is large, because the noise is averaged out by the summation over the many sensors, as expected from the law of large numbers. This is illustrated for example in [12], where it is also shown how KM fails to image in heterogeneous (cluttered) media. KM images in such media are unreliable and difficult to interpret because of the significant wave distortion by the inhomogeneities. The distortion is very different from additive, uncorrelated noise, and it cannot be reduced by simply summing over the sensors in the array. CINT images efficiently in clutter [8, 9, 10], at ranges that do not exceed one or two transport mean free paths [20]. Beyond such ranges the problem becomes much more difficult, specially in the case of active arrays, because the clutter backscatter overwhelms the echoes from the reflectors that we wish to image. Coherent imaging in such media may work only after pre-processing the data with filters of clutter backscatter, as is done in [12, 2]. The clutter considered in this paper is not as strong as in [12, 2], so imaging with CINT alone, without any extra array data filtering, gives good results.

The CINT method has been introduced in [8, 9, 10] for mitigating wave distortion effects induced by clutter. It forms images by superposing time delayed, local cross-correlations of the wave fields received at

*Computational and Applied Mathematics, Rice University, Houston, TX 77005. (borcea@caam.rice.edu)

†Laboratoire de Probabilités et Modèles Aléatoires & Laboratoire Jacques-Louis Lions, Université Paris VII, Site Chevaleret, 75205 Paris Cedex 13, France. (garnier@math.jussieu.fr)

‡Mathematics, Stanford University, Stanford, CA 94305. (papanicolaou@stanford.edu)

§Applied Mathematics, University of Crete and IACM/FORTH, GR-71409 Heraklion, Greece. (tsogka@tem.uoc.gr)

the array. Here local cross correlations means that they are computed in appropriate time windows and over limited array sensor offsets. It has been shown with analysis and verified with numerical simulations [8, 9, 10, 11, 7] that the time and offset thresholding in the computation of the cross-correlations is essential in CINT, because it introduces a smoothing that is necessary to achieve statistical stability, at the expense of some loss in resolution. By statistical stability we mean negligibly small fluctuations in the CINT image even when cumulative fluctuation effects in the random medium are not small.

The statistical stability of CINT has been studied analytically in [9, 11] using the paraxial wave approximation that neglects back scattering in random media. However, a detailed comparative study between KM and CINT has not been carried out because the scattering model in [9, 11] is too complicated to allow an analysis of the SNR.

In this paper we consider the resolution versus statistical stability trade-off in CINT using a relatively simple random travel time model for the effects of the random medium. We compute the mean and SNR* of the KM and CINT point spread functions, and show explicitly that no matter how large the array is, KM loses statistical stability at an exponential rate with the distance of propagation, the range. CINT is superior to KM because its SNR does not decay with range and it can be improved by increasing the array aperture.

The random travel time model [21, 19] captures wavefront distortions in heterogeneous media, but not the delay spread (coda) due to multiple scattering. The model is valid in the geometrical optics regime in random media with weak fluctuations and large correlation lengths compared to the wavelength [21, 19, 23, 15]. It ignores diffraction and amplitude fluctuations that cause scintillation, and it is widely used in adaptive optics for approximating wavefront distortions due to propagation in turbulent media [22, 16]. We use it in this paper because it allows us to carry out analytically a comparative study of resolution and statistical stability of CINT and KM.

The paper is organized as follows: We begin in section 2 with the statement of the array imaging problem and the mathematical expression of the KM and CINT imaging functions for passive and active arrays. The random travel time model is considered in section 3 with details of its derivation provided for completeness in Appendix A. We study the point spread function in passive array imaging in section 4. The resolution and stability analysis of KM is in section 4.3 and that of CINT in section 4.4. In section 5 we study active array imaging. We illustrate the analytical results with numerical simulations in section 6. We end with a summary in section 7.

2. Formulation of the array imaging problem. To image sources or reflectors in a medium we record the wave fields at a remote array of sensors. By an array we mean a collection of N sensors that are placed sufficiently close together to behave as a continuum aperture, the array. The basic propagation model is the scalar (acoustic) wave equation in $n+1$ dimensions, where $n = 1, 2$, and the array data consists of measurements of the acoustic pressure p. We refer to the measurements as *time traces* to emphasize that they are functions of time t.

2.1. Imaging with passive arrays. In the source localization problem the sensors are receivers and the array is called passive. The excitation comes from the unknown source and the receivers at $\vec{\boldsymbol{x}}_r$, for $r = 1, \ldots, N$, record the traces $p(t, \vec{\boldsymbol{x}}_r)$. Since we study the point spread function, we assume a point source

*The SNR is defined as the mean value of the imaging function at its peak, divided by its standard deviation.

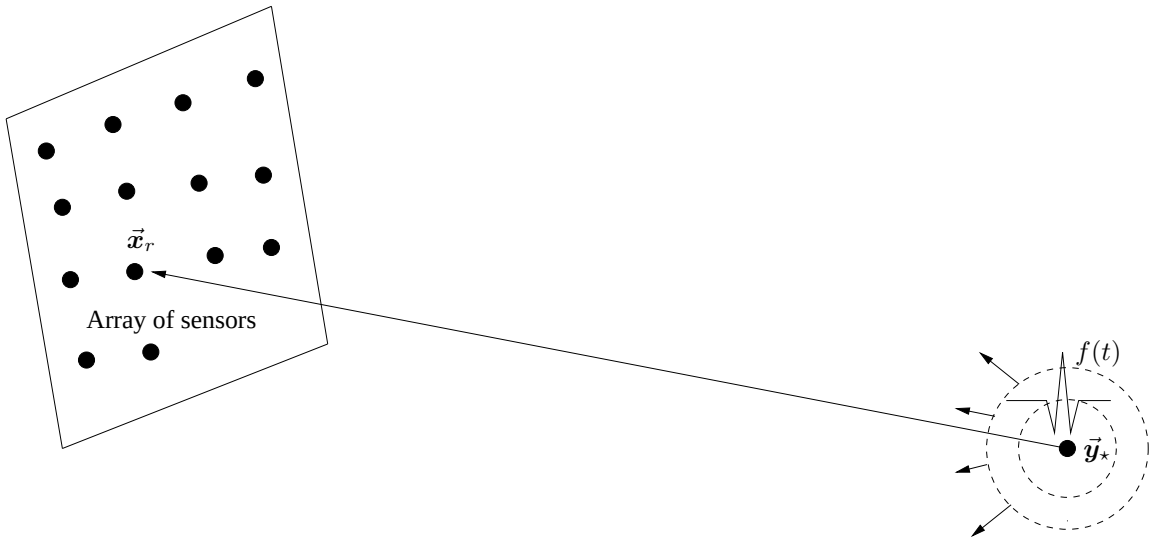

FIG. 2.1. *Setup for source localization with a passive array.*

at location $\vec{\boldsymbol{y}}$, as illustrated in Figure 2.1. It emits a pulse

$$f(t) = e^{-i\omega_o t} f_B(t), \tag{2.1}$$

with Fourier transform

$$\widehat{f}(\omega) = \int_{-\infty}^{\infty} dt\, f(t) e^{i\omega t} = \widehat{f}_B(\omega - \omega_o). \tag{2.2}$$

Here ω_o is the central frequency, f_B is the baseband pulse, and B denotes the bandwidth, that is, the size of the frequency interval that supports $\widehat{f}_B$. We take for convenience a Gaussian shaped pulse $f_B(t) = e^{-B^2t^2/2}$, so that we can evaluate explicitly the integrals that arise in the analysis and obtain explicit relations for the resolution and the SNR of CINT and KM. We have

$$f(t) = e^{-i\omega_o t - \frac{B^2t^2}{2}}, \qquad \widehat{f}(\omega) = \frac{\sqrt{2\pi}}{B} e^{-\frac{(\omega-\omega_o)^2}{2B^2}}, \tag{2.3}$$

and we assume that the width of $f(t)$, which scales as $1/B$, is much smaller than the travel time of the waves from the source to the array.

The inverse problem is to determine the location $\vec{\boldsymbol{y}}$ of the source from the array data traces, modeled by the convolution of the pulse with the Green's function $G(t, \vec{\boldsymbol{x}}_r, \vec{\boldsymbol{y}})$ of the wave equation

$$p(t, \vec{\boldsymbol{x}}_r) = f(t) \star G(t, \vec{\boldsymbol{x}}_r, \vec{\boldsymbol{y}}) = \int_{-\infty}^{\infty} \frac{d\omega}{2\pi}\, \widehat{f}(\omega) \widehat{G}(\omega, \vec{\boldsymbol{x}}_r, \vec{\boldsymbol{y}}) e^{-i\omega t}. \tag{2.4}$$

We analyze it using two imaging methods: KM and CINT. The KM imaging function is [5, 6]

$$\mathcal{I}^{\mathrm{KM}}(\vec{\boldsymbol{y}}^S) = \sum_{r=1}^{N} p(\tau_o(\vec{\boldsymbol{x}}_r, \vec{\boldsymbol{y}}^S), \vec{\boldsymbol{x}}_r) = \sum_{r=1}^{N} \int_{-\infty}^{\infty} \frac{d\omega}{2\pi}\, \widehat{p}(\omega, \vec{\boldsymbol{x}}_r) e^{-i\omega\tau_o(\vec{\boldsymbol{x}}_r, \vec{\boldsymbol{y}}^S)}, \tag{2.5}$$

where $\tau_o(\vec{\boldsymbol{x}}_r, \vec{\boldsymbol{y}}^S)$ is the travel time from the point $\vec{\boldsymbol{y}}^S$ at which we image to the receiver at $\vec{\boldsymbol{x}}_r$ in the background medium without fluctuations. In this paper we assume a homogeneous background medium and

so $\tau_o(\vec{\boldsymbol{x}}_r, \vec{\boldsymbol{y}}^S) = |\vec{\boldsymbol{x}}_r - \vec{\boldsymbol{y}}^S|/c_o$. In general τ_o is given by Fermat's principle. The KM function gives an image by superposing the time traces back propagated to $\vec{\boldsymbol{y}}^S$ with travel time delays.

The CINT imaging function [8, 9] is

$$\mathcal{I}^{\text{CINT}}(\vec{\boldsymbol{y}}^S) = \sum_{r,r'=1}^{N} \int_{-\infty}^{\infty} \frac{d\omega}{2\pi} \int_{-\infty}^{\infty} \frac{d\omega'}{2\pi} \widehat{\Phi}\left(\frac{\omega-\omega'}{\Omega_d}\right) \Psi\left(\frac{\vec{\boldsymbol{x}}_r - \vec{\boldsymbol{x}}_{r'}}{X_d}\right) \times \widehat{p}(\omega, \vec{\boldsymbol{x}}_r)\overline{\widehat{p}(\omega', \vec{\boldsymbol{x}}_{r'})} e^{-i\omega\tau_o(\vec{\boldsymbol{x}}_r, \vec{\boldsymbol{y}}^S) + i\omega'\tau_o(\vec{\boldsymbol{x}}_{r'}, \vec{\boldsymbol{y}}^S)}, \tag{2.6}$$

where the bar denotes complex conjugate and $\widehat{\Phi}$ and Ψ are windows with support scaled by two parameters Ω_d and X_d. We use these windows to threshold the frequency and sensor offsets over which we form cross-correlations of the array traces. In general, $\mathcal{I}^{\text{CINT}}$ does not have a simple expression in the time domain, like $\mathcal{I}^{\text{KM}}$, because the sensor offset threshold X_d may vary in the bandwidth [9]. If X_d were a constant, we could write

$$\mathcal{I}^{\text{CINT}}(\vec{\boldsymbol{y}}^S) = \sum_{r,r'=1}^{N} \Psi\left(\frac{\vec{\boldsymbol{x}}_r - \vec{\boldsymbol{x}}_{r'}}{X_d}\right) \int_{-\infty}^{\infty} dt\, \Omega_d \Phi\left(t\Omega_d\right) p\left(\tau_o(\vec{\boldsymbol{x}}_r, \vec{\boldsymbol{y}}^S) - t, \vec{\boldsymbol{x}}_r\right) \overline{p\left(\tau_o(\vec{\boldsymbol{x}}_{r'}, \vec{\boldsymbol{y}}^S) - t, \vec{\boldsymbol{x}}_{r'}\right)}.$$

This is somewhat similar to (2.5), but it forms the image by superposing the back propagated cross-correlations of the array traces over receivers that are not further than X_d apart and in a time interval scaled by $1/\Omega_d$. It is only when X_d is as large as the array aperture, and $\Omega_d \to \infty$, that the imaging methods become essentially the same, with $\mathcal{I}^{\text{CINT}}(\vec{\boldsymbol{y}}^S)$ proportional to $\left|\mathcal{I}^{\text{KM}}(\vec{\boldsymbol{y}}^S)\right|^2$.

The thresholding by X_d and Ω_d in the CINT imaging function (2.6) is essential when imaging in clutter. It introduces a smoothing in the imaging process that leads to statistically stable results, as shown in [11, 9] and with more analytical detail in this paper. The optimal thresholding is determined by the trade-off between the smoothing for stability and loss of resolution. The optimal parameters X_d and Ω_d are related to the decoherence length and frequency that describe how the wave fields lose coherence due to scattering in clutter. They may be determined directly from the data using statistical signal processing tools such as the variogram [17, 18], but the estimation may not be accurate enough. It is better to determine X_d and Ω_d adaptively during the image formation, as explained in [9].

2.2. Imaging with active arrays. The setup for imaging a reflector with an active array of sensors is illustrated in Figure 2.2. The reflector is centered at $\vec{\boldsymbol{y}}$ and the array is active, because its sensors play the dual role of sources and receivers. We denote the source locations by $\vec{\boldsymbol{x}}_s$ and the receivers by $\vec{\boldsymbol{x}}_r$. Even though s and r are indices that take integer values between 1 and N, we use them consistently in the paper to remind us which are the sources and receivers. We assume for simplicity that all the sources emit the same pulse $f(t)$ given by (2.3), and we denote the time traces recorded at the receivers by $p(t, \vec{\boldsymbol{x}}_r, \vec{\boldsymbol{x}}_s)$.

The imaging problem is to determine the support of the reflector from the array data traces. We study it using KM and CINT, and since we are interested in the point spread function, we assume that the reflector is a point at $\vec{\boldsymbol{y}}$ with reflectivity one. Then the model of the time traces is

$$p(t, \vec{\boldsymbol{x}}_r, \vec{\boldsymbol{x}}_s) = f(t) \star G(t, \vec{\boldsymbol{x}}_r, \vec{\boldsymbol{y}}) \star G(t, \vec{\boldsymbol{x}}_s, \vec{\boldsymbol{y}}) = \int_{-\infty}^{\infty} \frac{d\omega}{2\pi} \widehat{f}(\omega)\widehat{G}(\omega, \vec{\boldsymbol{x}}_r, \vec{\boldsymbol{y}})\widehat{G}(\omega, \vec{\boldsymbol{x}}_s, \vec{\boldsymbol{y}}) e^{-i\omega t}. \tag{2.7}$$

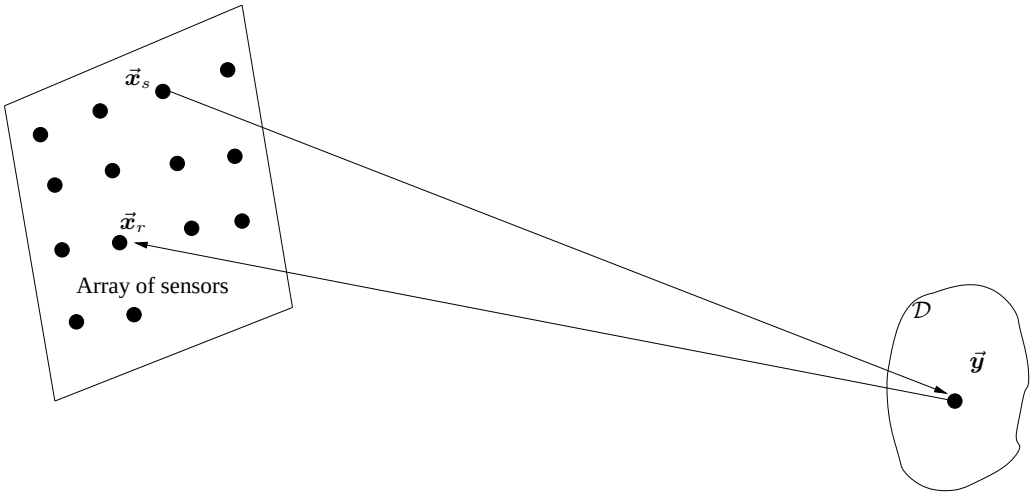

FIG. 2.2. *Setup for imaging with an active array.*

The KM imaging function with active arrays is

$$\begin{aligned}\mathcal{I}^{\mathrm{KM}}(\vec{\boldsymbol{y}}^S) &= \sum_{r,s=1}^{N} p(\tau_o(\vec{\boldsymbol{x}}_r,\vec{\boldsymbol{y}}^S)+\tau_o(\vec{\boldsymbol{x}}_s,\vec{\boldsymbol{y}}^S),\vec{\boldsymbol{x}}_r,\vec{\boldsymbol{x}}_s)\\ &= \sum_{r,s=1}^{N}\int_{-\infty}^{\infty}\frac{d\omega}{2\pi}\,\widehat{p}(\omega,\vec{\boldsymbol{x}}_r,\vec{\boldsymbol{x}}_s)e^{-i\omega\left[\tau_o(\vec{\boldsymbol{x}}_r,\vec{\boldsymbol{y}}^S)+\tau_o(\vec{\boldsymbol{x}}_s,\vec{\boldsymbol{y}}^S)\right]}. \end{aligned} \tag{2.8}$$

It is similar to (2.5) except that we sum over both the sources and receivers, and we account for the additional travel time between the source and the point $\vec{\boldsymbol{y}}^S$ at which we form the image.

The CINT imaging function is

$$\begin{aligned}\mathcal{I}^{\mathrm{CINT}}(\vec{\boldsymbol{y}}^S) = \sum_{s,s'=1}^{N}\sum_{r,r'=1}^{N}\int_{-\infty}^{\infty}\frac{d\omega}{2\pi}\int_{-\infty}^{\infty}\frac{d\omega'}{2\pi}\,\widehat{\Phi}\left(\frac{\omega-\omega'}{\Omega_d}\right)\Psi\left(\frac{\vec{\boldsymbol{x}}_r-\vec{\boldsymbol{x}}_{r'}}{X_d}\right)\Psi\left(\frac{\vec{\boldsymbol{x}}_s-\vec{\boldsymbol{x}}_{s'}}{X_d}\right)\\ \times\widehat{p}(\omega,\vec{\boldsymbol{x}}_r,\vec{\boldsymbol{x}}_s)\overline{\widehat{p}(\omega',\vec{\boldsymbol{x}}_{r'},\vec{\boldsymbol{x}}_{s'})}e^{-i\omega\left[\tau_o(\vec{\boldsymbol{x}}_r,\vec{\boldsymbol{y}}^S)+\tau_o(\vec{\boldsymbol{x}}_s,\vec{\boldsymbol{y}}^S)\right]+i\omega'\left[\tau_o(\vec{\boldsymbol{x}}_{r'},\vec{\boldsymbol{y}}^S)+\tau_o(\vec{\boldsymbol{x}}_{s'},\vec{\boldsymbol{y}}^S)\right]}. \end{aligned} \tag{2.9}$$

It forms the image with the superposition of the back propagated cross-correlations of the traces at sources and receivers that are not further than X_d apart.

2.3. Simplifying assumptions on the geometry, the array and the thresholding windows. We assume for simplicity that the array is in the plane $x_{n+1}=0$ in $\mathbb{R}^{n+1}$, where $n=1$ or 2. The center of the array is the origin of the system of coordinates, with axis x_{n+1} in the range direction, from the array to the point source or reflector that we wish to locate. The sensor locations are

$$\vec{\boldsymbol{x}}_r=(\boldsymbol{x}_r,0),\quad \boldsymbol{x}_r\in\mathcal{A}\subset\mathbb{R}^n,\quad r=1,\dots N, \tag{2.10}$$

and the unknown source or reflector location is

$$\vec{\boldsymbol{y}}=(\boldsymbol{y}=\boldsymbol{0},L). \tag{2.11}$$

Here L is the range and $\boldsymbol{y} \in \mathbb{R}^n$ is the cross-range. We take $\boldsymbol{y}$ at the origin to obtain simpler formulas. The results extend to $\boldsymbol{y} \neq \mathbf{0}$. The image points

$$\vec{\boldsymbol{y}}^S = (\boldsymbol{\xi}, L + \eta) \tag{2.12}$$

are offset from $\vec{\boldsymbol{y}}$ by $\boldsymbol{\xi}$ in cross-range and by η in range.

The sensors are uniformly spaced in $\mathcal{A} \subset \mathbb{R}^n$ at distance $h = a/N^{1/n}$ apart, and we suppose that N is large enough to be able to approximate the array by a continuum aperture. This allows us to approximate the sums over the sensors by integrals over $\mathcal{A}$,

$$\sum_{r=1}^{N} \rightsquigarrow \frac{1}{h^n} \int_{\mathcal{A}} d\boldsymbol{x}. \tag{2.13}$$

We use henceforth this continuum approximation and we drop the scaling constant h^{-n}. In three dimensions, where $n = 2$, $\mathcal{A}$ is the square with center at $\mathbf{0}$ of side a, the array aperture. $\mathcal{A}$ is the interval $[-a/2, a/2]$ in two dimensions, where $n = 1$.

For simplicity in the analysis of CINT, we take Gaussian shaped thresholding windows

$$\Phi(t) = e^{-t^2/2}, \qquad \Psi\big(\vec{\boldsymbol{x}} = (\boldsymbol{x}, 0)\big) = e^{-|\boldsymbol{x}|^2/2}. \tag{2.14}$$

Just as the Gaussian assumption (2.3) on the pulse, (2.14) allows us to evaluate analytically the integrals in $\mathcal{I}^{\text{CINT}}$ to obtain explicit expressions of its mean and SNR.

3. The noise and random travel time model. The Green's function $G(t, \vec{\boldsymbol{x}}_r, \vec{\boldsymbol{y}})$ in equations (2.4) and (2.7) is for the wave equation in a random medium, with wave speed $c(\vec{\boldsymbol{x}})$ defined by

$$\frac{1}{c^2(\vec{\boldsymbol{x}})} = \frac{1}{c_o^2} \left[1 + \sigma \mu \left(\frac{\vec{\boldsymbol{x}}}{\ell} \right) \right]. \tag{3.1}$$

It fluctuates about the constant speed c_o, as modeled with the random, mean zero function μ. We assume that μ is statistically homogeneous with autocorrelation

$$\mathcal{R}(\vec{\boldsymbol{x}} - \vec{\boldsymbol{x}}') = \mathbb{E}\left\{ \mu(\vec{\boldsymbol{x}}) \mu(\vec{\boldsymbol{x}}') \right\}, \tag{3.2}$$

normalized so that $\mathcal{R}(\mathbf{0}) = 1$ and

$$\int_{\mathbb{R}^{n+1}} d\vec{\boldsymbol{x}}\, \mathcal{R}(\vec{\boldsymbol{x}}) = O(1). \tag{3.3}$$

The strength of the fluctuations is quantified by σ, and under the assumption that the power spectral density of the fluctuations (the Fourier transform of the covariance function $\mathcal{R}$) decays fast, the effective correlation length is given by ℓ. We take henceforth for simplicity, and without loss of generality, a Gaussian autocorrelation for μ,

$$\mathcal{R}(\vec{\boldsymbol{x}}) = e^{-|\vec{\boldsymbol{x}}|^2/2}. \tag{3.4}$$

The travel time is given by Fermat's principle

$$\tau(\vec{\boldsymbol{x}}, \vec{\boldsymbol{y}}) = \min_{\Gamma} \int_{\Gamma} \frac{du}{c(\vec{\boldsymbol{x}}(u))}, \tag{3.5}$$

where Γ denotes the paths from $\vec{\boldsymbol{y}}$ to $\vec{\boldsymbol{x}}$, parametrized by the arclength u. It fluctuates randomly about the value

$$\tau_o(\vec{\boldsymbol{x}}, \vec{\boldsymbol{y}}) = \frac{|\vec{\boldsymbol{x}} - \vec{\boldsymbol{y}}|}{c_o}, \tag{3.6}$$

which is the travel time in the homogeneous background.

We consider waves that travel long distances

$$\ell \ll L. \tag{3.7}$$

We assume further that the random fluctuations of the wave speed are weak

$$\sigma^2 \ll \frac{\ell^3}{L^3}, \tag{3.8}$$

and that the typical wavelength λ (where $\omega = 2\pi c_o/\lambda$) satisfies

$$\sigma^2 \frac{L^3}{\ell^3} \ll \frac{\lambda^2}{\sigma^2 \ell L} \lesssim 1. \tag{3.9}$$

The three conditions (3.7-3.8-3.9) ensure the validity of the random travel time model, which is a special high-frequency model $\lambda \ll l$ in which the reciprocal of the Fresnel number relative to the correlation length is small

$$\frac{L\lambda}{\ell^2} \lesssim \frac{\sigma L^{3/2}}{\ell^{3/2}} \ll 1.$$

In this model the geometric optics approximation is valid in the presence of random fluctuations of the wave speed. The perturbation of the amplitude of the propagating waves is negligible, while the perturbation of the phase of the waves is of order one or larger, and described in terms of Gaussian statistics. The range of validity of this model is analyzed in Appendix A in terms of the conditions (3.7-3.8-3.9). We note that:

- The condition $\ell \ll L$ ensures that the fluctuations of the travel time have approximately Gaussian statistics by invoking the central limit theorem.
- The term $\sigma^2(L/\ell)^3$ quantifies the variance of the fluctuations of the amplitude of the waves, so it should be small to ensure that the perturbation of the amplitude is negligible.
- The term $\sigma^2 \ell L/\lambda^2$ quantifies the variance of the fluctuations of the phase of the waves, so it should be large enough to ensure that the perturbation of the phase is not negligible.

Similar conditions for the validity of the random travel time model can be found in [21, Chapter 6], [19, Chapter 1] and in [15].

The random travel time model provides an approximate expression for the Green's function between two points at a distance of order L from each other

$$\widehat{G}(\omega, \vec{\boldsymbol{x}}, \vec{\boldsymbol{y}}) \approx \alpha_o(|\vec{\boldsymbol{x}} - \vec{\boldsymbol{y}}|, \omega) e^{i\omega[\tau_o(\vec{\boldsymbol{x}}, \vec{\boldsymbol{y}}) + \nu_\tau(\vec{\boldsymbol{x}}, \vec{\boldsymbol{y}})]}. \tag{3.10}$$

Here α_o is the amplitude of the Green's function in the background medium, which is uniform in our case, and $\nu_\tau(\vec{\boldsymbol{x}}, \vec{\boldsymbol{y}})$ is the random travel time perturbation given by the integral of the fluctuations of $1/c$ along the unperturbed, straight ray from $\vec{\boldsymbol{y}}$ to $\vec{\boldsymbol{x}}$,

$$\nu_\tau(\vec{\boldsymbol{x}}, \vec{\boldsymbol{y}}) = \frac{\sigma|\vec{\boldsymbol{x}} - \vec{\boldsymbol{y}}|}{2c_o} \int_0^1 ds\, \mu\left(\frac{\vec{\boldsymbol{y}} + (\vec{\boldsymbol{x}} - \vec{\boldsymbol{y}})s}{\ell}\right). \tag{3.11}$$

Since the source point $\vec{\boldsymbol{y}}$ is at long range from the array ($L \gg \ell$), the statistical distribution of the travel time perturbation $\nu_\tau(\vec{\boldsymbol{x}}, \vec{\boldsymbol{y}})$ takes the form described in the following lemma.

LEMMA 3.1. *If $\vec{\boldsymbol{y}} = (\boldsymbol{0}, L) \in \mathbb{R}^{n+1}$ and $\mathcal{A} \subset \mathbb{R}^n$ with diam($\mathcal{A}$) $\ll L$, $\ell \ll L$, then the random process defined for $\boldsymbol{x} \in \mathcal{A}$ by*

$$\nu(\boldsymbol{x}) := \nu_\tau\big(\vec{\boldsymbol{x}} = (\boldsymbol{x}, 0), \vec{\boldsymbol{y}}\big) \tag{3.12}$$

has Gaussian statistics with mean zero and covariance function

$$\mathbb{E}\left\{\nu(\boldsymbol{x})\nu(\boldsymbol{x}')\right\} = \tau_c^2 \mathcal{C}\left(\frac{|\boldsymbol{x} - \boldsymbol{x}'|}{\ell}\right). \tag{3.13}$$

Here

$$\tau_c^2 = \frac{\sqrt{2\pi}\sigma^2 \ell L}{4c_o^2} \tag{3.14}$$

is the variance of the random travel time fluctuations and

$$\mathcal{C}(r) = \frac{1}{r}\int_0^r du\, e^{-u^2/2} \tag{3.15}$$

is the normalized form of the covariance.

Proof. It follows by direct calculation from (3.11), (3.4) and the assumption $L \gg |\boldsymbol{x}|, |\boldsymbol{x}'|$ that the random process $\nu(\boldsymbol{x})$ has mean zero and covariance function

$$\begin{aligned}\mathbb{E}\left\{\nu(\boldsymbol{x})\nu(\boldsymbol{x}')\right\} &= \frac{\sigma^2 L^2}{4c_o^2}\int_0^1 ds \int_0^1 ds' \exp\left[-\frac{|s(\boldsymbol{x}-\boldsymbol{x}') + (s-s')\boldsymbol{x}'|^2}{2\ell^2} - \frac{(s-s')^2 L^2}{2\ell^2}\right] \\ &= \frac{\sigma^2 L^2}{4c_o^2}\int_0^1 ds \int_{-s}^{1-s} d\tilde{s} \exp\left[-\frac{|s(\boldsymbol{x}-\boldsymbol{x}') - \tilde{s}\boldsymbol{x}'|^2}{2\ell^2} - \frac{\tilde{s}^2 L^2}{2\ell^2}\right].\end{aligned} \tag{3.16}$$

The Gaussian property is automatic if μ is Gaussian. In the general case the Gaussian property is obtained from a form of the central limit theorem when $L \gg \ell$. Moreover, when $L \gg \ell$, we can extend the $\tilde{s}$ integral in (3.16) to the entire real line, to obtain (3.13-3.14). □

The analysis of the KM and CINT imaging functions involves the computation of statistical moments of the Green's function. These moments follow from (3.13) and the Gaussianity of ν.

LEMMA 3.2. *If $\boldsymbol{y} = (\boldsymbol{0}, L) \in \mathbb{R}^{n+1}$ and $\mathcal{A} \subset \mathbb{R}^n$ with diam($\mathcal{A}$) $\ll L$, $\ell \ll L$, then we have (approximately)*

$$\mathbb{E}\left\{e^{i\omega\nu(\boldsymbol{x})}\right\} = exp\left\{-\frac{\omega\tau_c^2}{2}\right\}, \tag{3.17}$$

$$\mathbb{E}\left\{e^{i\omega\nu(\boldsymbol{x}) - i\omega'\nu(\boldsymbol{x}')}\right\} = exp\left\{-\frac{(\omega-\omega')^2\tau_c^2}{2} - \omega\omega'\tau_c^2\left[1 - \mathcal{C}\left(\frac{|\boldsymbol{x}-\boldsymbol{x}'|}{\ell}\right)\right]\right\}. \tag{3.18}$$

If, additionally, $\omega\tau_c, \omega'\tau_c \gg 1$, then

$$\mathbb{E}\left\{e^{i\omega\nu(\boldsymbol{x}) - i\omega'\nu(\boldsymbol{x}')}\right\} \approx exp\left\{-\frac{(\omega-\omega')^2}{2\Omega_c^2} - \frac{|\boldsymbol{x}-\boldsymbol{x}'|^2}{2X_c^2}\right\}, \tag{3.19}$$

where

$$X_c = \frac{\sqrt{3}\ell}{\omega_o\tau_c}, \qquad \Omega_c = \frac{1}{\tau_c}. \tag{3.20}$$

Equation (3.19) means that X_c is the decoherence length of the Green's function for receiving points in $\mathcal{A}$ and Ω_c is its decoherence frequency. Note that the additional condition $\omega\tau_c \gg 1$ is equivalent to having $\frac{\lambda^2}{\sigma^2 \ell L} \ll 1$ in (3.9).

Proof. Equations (3.17-3.18) follow from the expression of the characteristic function of a Gaussian random variable

$$\mathbb{E}\left\{e^{i\omega\nu(\boldsymbol{x})-i\omega'\nu(\boldsymbol{x}')}\right\} = \exp\left\{-\frac{\mathbb{E}\left\{[\omega\nu(\boldsymbol{x})-\omega'\nu(\boldsymbol{x}')]^2\right\}}{2}\right\}.$$

When $\omega\tau_c, \omega'\tau_c \gg 1$ the first order moment (3.17) is very small, and so is the second-order moment (3.18) for $|\boldsymbol{x}-\boldsymbol{x}'| \geq \ell$. It is only for $|\boldsymbol{x}-\boldsymbol{x}'| \ll \ell$, where $\mathcal{C}\left(|\boldsymbol{x}-\boldsymbol{x}'|/\ell\right) \approx 1$, that the expectation in (3.18) is of order one. We can then expand the covariance function (3.15) around zero: $\mathcal{C}(r) = 1 - r^2/6 + o(r^2)$ to get the result (3.19-3.20). □

Consider for example the mean of the Green's function

$$\mathbb{E}\left\{\widehat{G}(\omega,\vec{\boldsymbol{x}},\vec{\boldsymbol{y}})\right\} = G_o(\omega,\vec{\boldsymbol{x}},\vec{\boldsymbol{y}})\mathbb{E}\left\{e^{i\omega\nu(\boldsymbol{x})}\right\} = \widehat{G}_o(\omega,\vec{\boldsymbol{x}},\vec{\boldsymbol{y}})e^{-\frac{\omega^2\tau_c^2}{2}}, \tag{3.21}$$

and its variance

$$\mathbb{E}\left\{|\widehat{G}(\omega,\vec{\boldsymbol{x}},\vec{\boldsymbol{y}})|^2\right\} - \left|\mathbb{E}\left\{\widehat{G}(\omega,\vec{\boldsymbol{x}},\vec{\boldsymbol{y}})\right\}\right|^2 = \left|\widehat{G}_o(\omega,\vec{\boldsymbol{x}},\vec{\boldsymbol{y}})\right|^2\left(1-e^{-\omega^2\tau_c^2}\right). \tag{3.22}$$

We see that $\widehat{G} \approx \widehat{G}_o$ in very weak clutter $\omega\tau_c \ll 1$, where the wavefront distortions are negligible. In this paper we study the regime with strong wavefront distortions, where $\omega\tau_c \gg 1$ and $\widehat{G}$ has significant random phase fluctuations.

4. Source localization with passive arrays. We study in section 4.3 the mean and variance of the KM imaging function. The analysis of CINT and the comparison with KM is in section 4.4. The scaling regime and the data model are described in sections 4.1-4.2.

4.1. Scaling assumptions on the array and the source. The pulse width, which scales like $1/B$, is assumed short compared to typical travel times, as stated in section 2.1, but we take

$$B \ll \omega_o, \tag{4.1}$$

so that all the wavelengths are close to the central one λ_o.

The array aperture a may be larger or similar to ℓ, and it satisfies

$$\theta = \frac{a^2}{\lambda_o L} \gg 1. \tag{4.2}$$

Here θ is the array Fresnel number and the assumption says that the aperture is large with respect to the focal spot size $\lambda_o L/a$, which is the first zero of the array diffraction pattern in the Fraunhofer diffraction regime [13, Chapter 8.5]. The aperture is small with respect to the range L, and in fact we suppose that

$$\frac{a}{L} \ll \frac{1}{\sqrt{\theta}} \ll 1, \tag{4.3}$$

so that we can approximate the background phase from the source $\vec{\boldsymbol{y}}$ to the receiver $\vec{\boldsymbol{x}}_r$ by

$$\omega\tau_o(\vec{\boldsymbol{x}}_r,\vec{\boldsymbol{y}}) = \frac{\omega}{c}\left(L + \frac{|\boldsymbol{x}_r|^2}{2L}\right) + o(1), \tag{4.4}$$

with negligible residual in the regime of interest.

The image domain (with image points of the form (2.12)) is much larger than the spot size $\lambda_o L/a$ in cross-range and c/B in range, in order to observe the focus. However, we bound it by

$$|\boldsymbol{\xi}| \ll \min\left\{\sqrt{\lambda_o L}, \frac{\omega_o}{B}\frac{\lambda_o L}{a}\right\}, \qquad |\eta| \ll \frac{L}{\theta} \ll L, \tag{4.5}$$

to obtain the following approximation for the background phase from the image point $\vec{\boldsymbol{y}}^S$ to the receiver $\vec{\boldsymbol{x}}_r$

$$\omega\tau_o(\vec{\boldsymbol{x}}_r, \vec{\boldsymbol{y}}^S) = \frac{\omega}{c}\left(L + \eta + \frac{|\boldsymbol{x}_r|^2}{2L}\right) - \frac{\omega_o}{c}\frac{\boldsymbol{x}_r \cdot \boldsymbol{\xi}}{L} + o(1). \tag{4.6}$$

4.2. The data set. The data set (2.4) in the frequency domain is of the form

$$\hat{p}(\omega, \vec{\boldsymbol{x}}_r) = \widehat{f}(\omega)\widehat{G}(\omega, \vec{\boldsymbol{x}}_r, \vec{\boldsymbol{y}}) \approx \widehat{P}(\omega, \boldsymbol{x}_r) := \widehat{f}(\omega)\alpha_o(L, \omega_o)e^{i\omega\tau_o(\vec{\boldsymbol{x}}_r, \vec{\boldsymbol{y}}) + i\omega\nu(\boldsymbol{x}_r)}, \tag{4.7}$$

where we used (3.10) and (3.12). Since $\vec{\boldsymbol{x}}_r = (\boldsymbol{x}_r, 0)$, we suppressed the constant zero range in the arguments of $\widehat{P}$. The statistical distribution of ν is Gaussian as described in Lemma 3.1. The smooth amplitude α_o of the background Green's function is approximated by

$$\alpha_o(|\vec{\boldsymbol{x}} - \vec{\boldsymbol{y}}|, \omega) \approx \alpha_o(L, \omega_o), \tag{4.8}$$

because $a \ll L$ and the bandwidth is much smaller than ω_o. Thus,

$$\widehat{G}_o(\omega, \vec{\boldsymbol{x}}, \vec{\boldsymbol{y}}) \approx \alpha_o(L, \omega_o)e^{i\omega\tau_o(\vec{\boldsymbol{x}}, \vec{\boldsymbol{y}})} \tag{4.9}$$

is the approximate Green's function in the homogeneous background, with travel time τ_o given by (3.6) and amplitude

$$\alpha_o(L, \omega_o) = \begin{cases} \frac{1}{4\pi L} & \text{if } n = 2, \\ \frac{1}{2}\sqrt{\frac{ic_o}{2\pi L\omega_o}} & \text{if } n = 1. \end{cases} \tag{4.10}$$

4.3. Kirchhoff migration imaging. The KM imaging function with passive arrays is

$$\begin{aligned} \mathcal{I}^{\mathrm{KM}}(\vec{\boldsymbol{y}}^S) &= \int_{\mathcal{A}} d\boldsymbol{x}_r \int_{-\infty}^{\infty} \frac{d\omega}{2\pi}\, \widehat{P}(\omega, \boldsymbol{x}_r)e^{-i\omega\tau_o(\vec{\boldsymbol{x}}_r, \vec{\boldsymbol{y}}^S)} \\ &\approx \alpha_o(L, \omega_o) \int_{\mathcal{A}} d\boldsymbol{x}_r \int_{-\infty}^{\infty} \frac{d\omega}{2\pi}\, \widehat{f}(\omega) \exp\left\{-i\frac{\omega}{c_o}\eta + i\frac{\omega_o}{c_o}\frac{\boldsymbol{\xi} \cdot \boldsymbol{x}_r}{L} + i\omega\nu(\boldsymbol{x}_r)\right\}, \end{aligned} \tag{4.11}$$

where we used the data model (4.7) and approximations (4.4) and (4.6).

4.3.1. Homogeneous media. If there are no fluctuations, we have from (4.11) with $\nu = 0$, after integrating over frequency and aperture, that the point spread function is

$$\begin{aligned} \mathcal{I}_o^{\mathrm{KM}}(\vec{\boldsymbol{y}}^S) &\approx a^n \alpha_o(L, \omega_o) \prod_{j=1}^{n} \mathrm{sinc}\left(\frac{\pi a\xi_j}{\lambda_o L}\right) f\left(\frac{\eta}{c_o}\right) \\ &= a^n \alpha_o(L, \omega_o) \prod_{j=1}^{n} \mathrm{sinc}\left(\frac{\pi a\xi_j}{\lambda_o L}\right) e^{-i\frac{\omega_o}{c_o}\eta - \frac{B^2\eta^2}{2c_o^2}}. \end{aligned} \tag{4.12}$$

It peaks at $\vec{\boldsymbol{y}}^S = \vec{\boldsymbol{y}}$, where $\boldsymbol{\xi} = (\xi_1, \ldots, \xi_n) = \mathbf{0}$ and $\eta = 0$. The range resolution is determined by the width $1/B$ of the pulse,

$$|\eta| \lesssim \frac{c_o}{B}, \tag{4.13}$$

where we use symbol $\lesssim$ to indicate that there is a multiplicative, order one constant in the bound. The cross-range resolution, defined as the radial distance from the peak to the first zero, is

$$|\boldsymbol{\xi}| \leq \frac{\lambda_o L}{a}, \tag{4.14}$$

which is the classical Rayleigh resolution formula [13].

4.3.2. Random media. The imaging function (4.11) is random, with mean

$$\mathbb{E}\left\{\mathcal{I}^{\text{KM}}(\vec{\boldsymbol{y}}^S)\right\} \approx a^n \alpha_o(L, \omega_o) \prod_{j=1}^{n} \text{sinc}\left(\frac{\pi a \xi_j}{\lambda_o L}\right) \int_{-\infty}^{\infty} \frac{d\omega}{2\pi}\, \widehat{f}(\omega) \exp\left\{-i\frac{\omega}{c_o}\eta - \frac{\omega^2 \tau_c^2}{2}\right\}.$$

Here we use (3.21) and compute the integral over the aperture. Using also the Gaussian pulse shape (2.3), we obtain

$$\mathbb{E}\left\{\mathcal{I}^{\text{KM}}(\vec{\boldsymbol{y}}^S)\right\} \approx a^n \alpha_o(L, \omega_o) D \prod_{j=1}^{n} \text{sinc}\left(\frac{\pi a \xi_j}{\lambda_o L}\right) e^{-i\frac{\omega_o}{c_o}\frac{\eta}{(1+B^2\tau_c^2)} - \frac{B^2\eta^2}{2c_o^2(1+B^2\tau_c^2)}}, \tag{4.15}$$

where

$$D = \frac{\exp\left[-\frac{\omega_o^2\tau_c^2}{2(1+B^2\tau_c^2)}\right]}{\sqrt{1+B^2\tau_c^2}} \tag{4.16}$$

captures the strong damping effect on the mean waves by the random medium.

We see that the mean of the KM imaging function peaks at the true location $\vec{\boldsymbol{y}}$, where the offsets $\boldsymbol{\xi}$ and η are zero. The cross-range resolution is the same as in the homogeneous medium. However, the range resolution

$$|\eta| \lesssim \frac{c_o}{B}\sqrt{1+\tau_c^2 B^2} \tag{4.17}$$

deteriorates as $B\tau_c$ grows. This is because as we change the realizations of the medium, the peak dances around the zero range offset, due to the random travel time perturbations scaled by τ_c. When we average, we essentially see the envelope of these random point spread functions, which can be significantly smeared in range depending on how large $B\tau_c$ is.

In addition to the blur in range, there is a strong exponential damping of the mean point spread function, as seen from (4.16). This implies that $\mathcal{I}^{\text{KM}}(\vec{\boldsymbol{y}}^S)$ is essentially incoherent, with its random fluctuations dominating the mean, as follows more clearly from the relative standard deviation at its peak, given in the following proposition.

PROPOSITION 4.1. *The peak of* $\mathbb{E}\left\{\mathcal{I}^{KM}(\vec{\boldsymbol{y}}^S)\right\}$ *is at* $\vec{\boldsymbol{y}}^S = \vec{\boldsymbol{y}}$ *but it is strongly damped,*

$$\mathbb{E}\left\{\mathcal{I}^{KM}(\vec{\boldsymbol{y}})\right\} = \frac{\mathcal{I}_o^{KM}(\vec{\boldsymbol{y}})}{\sqrt{1+B^2\tau_c^2}} e^{-\frac{\omega_o^2\tau_c^2}{2(1+B^2\tau_c^2)}}. \tag{4.18}$$

The fluctuations do not experience such a damping,

$$\mathbb{E}\left\{|\mathcal{I}^{KM}(\vec{\boldsymbol{y}})|^2\right\} \approx |\mathcal{I}_o^{KM}(\vec{\boldsymbol{y}})|^2 \left(\frac{\sqrt{2\pi}X_c}{a}\right)^n \left(1+2B^2\tau_c^2\right)^{-\frac{1}{2}}, \tag{4.19}$$

where the approximation sign means equality up to an $1+o(1)$ factor, and the decoherence length X_c is given by (3.20). Therefore, the SNR is small

$$SNR^{KM} = \frac{|\mathbb{E}\{\mathcal{I}^{KM}(\vec{\boldsymbol{y}})\}|}{\sqrt{Var\{\mathcal{I}^{KM}(\vec{\boldsymbol{y}})\}}} \approx \left(\frac{a}{\sqrt{2\pi}X_c}\right)^{\frac{n}{2}} \frac{\left(1+2B^2\tau_c^2\right)^{1/4}}{\left(1+B^2\tau_c^2\right)^{1/2}} e^{-\frac{\omega_o^2\tau_c^2}{2(1+B^2\tau_c^2)}} \tag{4.20}$$

and decreases exponentially with $(\omega_o\tau_c)^2 \gg 1$.

Proof. Equation (4.18) follows easily from (4.15) and (4.12). The second-order moment calculation is in Appendix B. It uses (3.18) and (3.19). Since the mean is exponentially small, (4.19) approximates the variance

$$\mathrm{Var}\left\{\mathcal{I}^{\mathrm{KM}}(\vec{\boldsymbol{y}})\right\} = \mathbb{E}\left\{\left|\mathcal{I}^{\mathrm{KM}}(\vec{\boldsymbol{y}})\right|^2\right\} - \left|\mathbb{E}\left\{\mathcal{I}^{\mathrm{KM}}(\vec{\boldsymbol{y}})\right\}\right|^2.$$

The SNR is obtained from (4.18) and (4.19) by direct calculation. □

4.4. Coherent interferometric imaging. The CINT point spread function for passive arrays is

$$\begin{aligned}\mathcal{I}^{\mathrm{CINT}}(\vec{\boldsymbol{y}}^S) = \int_{\mathcal{A}} d\boldsymbol{x}_r \int_{\mathcal{A}} d\boldsymbol{x}_r' \int_{-\infty}^{\infty} \frac{d\omega}{2\pi} \int_{-\infty}^{\infty} \frac{d\omega'}{2\pi} \widehat{P}(\omega, \boldsymbol{x}_r)\overline{\widehat{P}(\omega', \boldsymbol{x}_r')}\widehat{\Phi}\left(\frac{\omega-\omega'}{\Omega_d}\right)\Psi\left(\frac{\boldsymbol{x}_r-\boldsymbol{x}_r'}{X_d}\right) \\ \times \exp\left\{-i\frac{(\omega-\omega')}{c_o}(L+\eta) + i\frac{\omega_o}{c_o}\frac{\boldsymbol{\xi}\cdot(\boldsymbol{x}_r-\boldsymbol{x}_r')}{L} - i\frac{\omega}{c_o}\frac{|\boldsymbol{x}_r|^2}{2L} + i\frac{\omega'}{c_o}\frac{|\boldsymbol{x}_r'|^2}{2L}\right\},\end{aligned} \tag{4.21}$$

where we used approximation (4.6). The data model $\widehat{P}(\omega, \boldsymbol{x})$ is given by (4.7).

While in general it is advantageous to let X_d vary over the bandwidth [9, 11], in the asymptotic regime considered in this paper we may take it to be constant. This assumption, within the random travel time model, simplifies the calculations and is justified by the conclusion drawn below that the optimal thresholding is $X_d \sim X_c$, where the decoherence length (3.20) is constant.

4.4.1. CINT as the smoothed Wigner transform. To show how the thresholding windows $\widehat{\Phi}$ and Ψ introduce a smoothing in CINT, let us rewrite (4.21) in terms of the Wigner transform of $\widehat{P}$,

$$W(\omega, \boldsymbol{x}; \boldsymbol{\kappa}, T) = \int_{\mathbb{R}^n} d\widetilde{\boldsymbol{x}} \int_{-\infty}^{\infty} d\widetilde{\omega}\, \widehat{P}\left(\omega + \frac{\widetilde{\omega}}{2}, \boldsymbol{x} + \frac{\widetilde{\boldsymbol{x}}}{2}\right)\overline{\widehat{P}\left(\omega - \frac{\widetilde{\omega}}{2}, \boldsymbol{x} - \frac{\widetilde{\boldsymbol{x}}}{2}\right)} e^{i\boldsymbol{\kappa}\cdot\widetilde{\boldsymbol{x}} - i\widetilde{\omega}T}. \tag{4.22}$$

We have the following result proved in Appendix C.

PROPOSITION 4.2. *Assume that the thresholding parameters X_d and Ω_d in CINT are sufficiently small so that*

$$\frac{B}{\omega_o}\frac{X_d}{\lambda_o L/a} \ll 1, \qquad \frac{\Omega_d}{\omega_o}\frac{X_d^2}{\lambda_o L} \ll 1. \tag{4.23}$$

Then, the CINT imaging function is given by the Wigner transform smoothed over all its arguments,

$$\begin{aligned}\mathcal{I}^{CINT}(\vec{\boldsymbol{y}}^S) = \frac{\Omega_d X_d^n}{(2\pi)^{\frac{n+5}{2}}} \int_{\mathcal{A}} d\boldsymbol{x} \int_{-\infty}^{\infty} d\omega \int_{\mathbb{R}^n} d\boldsymbol{\kappa} \int_{-\infty}^{\infty} dT\, W(\omega, \boldsymbol{x}; \boldsymbol{\kappa}, T) \\ \times\, exp\left\{-\frac{\Omega_d^2\left[T - \tau_o(\vec{\boldsymbol{x}}, \vec{\boldsymbol{y}}^S)\right]^2}{2} - \frac{X_d^2\left|\boldsymbol{\kappa} - \frac{\omega_o}{c_o}\frac{(\boldsymbol{\xi}-\boldsymbol{x})}{L}\right|^2}{2}\right\}.\end{aligned} \tag{4.24}$$

This is essentially the same result as in [11], obtained there with the more complicated forward scattering or parabolic approximation model. Note how the thresholding over the frequency offsets results in smoothing over time T, by convolution with the Gaussian of standard deviation $1/\Omega_d$. The convolution is evaluated at the travel time $\tau_o(\vec{\boldsymbol{x}}, \vec{\boldsymbol{y}}^S)$, and the smaller Ω_d is the more smoothing there is. The thresholding over sensor offsets results in smoothing over directions, by convolution with the Gaussian of standard deviation $X_d\omega_o/c_o \sim X_d/\lambda_o$. Again, the smaller X_d is the more smoothing there is.

4.4.2. The mean of CINT. To calculate the mean of the point spread function (4.24), let us consider first the mean of the Wigner transform. It is derived in Appendix D, under the assumptions

$$\frac{1}{\omega_o\tau_c}\frac{X_c^2}{\lambda_o L} = \frac{3}{(\omega_o\tau_c)^3}\frac{\ell^2}{\lambda_o L} \ll 1, \qquad \frac{B}{\omega_o}\frac{X_c}{\lambda_o L/a} = \frac{\sqrt{3}}{\omega_o\tau_c}\frac{B}{\omega_o}\frac{\ell a}{\lambda_o L} \ll 1. \tag{4.25}$$

These assumptions follow from (4.23) if $\Omega_d \sim \tau_c^{-1}$ and $X_d \sim X_c$. We give them here to allow for the case where the thresholding parameters in CINT are different than the decoherence ones.

PROPOSITION 4.3. *The mean Wigner transform is given by*

$$\begin{aligned}\mathbb{E}\left\{W(\omega, \boldsymbol{x}; \boldsymbol{\kappa}, T)\right\} \approx |\alpha_o(L,\omega_o)|^2 \left|\widehat{f}(\omega)\right|^2 (2\pi)^{\frac{n+1}{2}} X_c^n \sqrt{\frac{2B^2}{1+2B^2\tau_c^2}} \\ \times exp\left\{-\frac{B^2\left[T-\tau_o(\vec{\boldsymbol{x}},\vec{\boldsymbol{y}})\right]^2}{1+2B^2\tau_c^2} - \frac{X_c^2\left|\boldsymbol{\kappa}+\frac{\omega_o}{c_o}\frac{\boldsymbol{x}}{L}\right|^2}{2}\right\}.\end{aligned} \tag{4.26}$$

The mean CINT point spread function $\mathbb{E}\{\mathcal{I}^{\rm CINT}(\vec{\boldsymbol{y}}^S)\}$ follows from (4.24) and Proposition 4.3, as shown in Appendix D.

PROPOSITION 4.4. *The mean CINT point spread function with passive arrays is given by*

$$\begin{aligned}\mathbb{E}\left\{\mathcal{I}^{CINT}(\vec{\boldsymbol{y}}^S)\right\} \approx |\alpha_o(L,\omega_o)|^2 (2\pi)^{\frac{n}{2}} a^{2n}\left(\frac{a^2}{X_c^2}+\frac{a^2}{X_d^2}\right)^{-n/2} \frac{\Omega_d/B}{\sqrt{2+2\Omega_d^2\tau_c^2+(\Omega_d/B)^2}} \\ \times exp\left\{-\frac{\Omega_d^2}{2\left[2+2\Omega_d^2\tau_c^2+(\Omega_d/B)^2\right]}\left(\frac{\eta}{c_o}\right)^2 - \frac{X_d^2X_c^2}{2(X_d^2+X_c^2)}\left(\frac{\omega_o}{c_o}\frac{|\boldsymbol{\xi}|}{L}\right)^2\right\}.\end{aligned} \tag{4.27}$$

We compare it to the mean KM point spread function in section 4.4.4.

4.4.3. The SNR of CINT. To study the SNR of CINT, we compute first its variance. We obtain, after a calculation given in Appendix E, the following result.

PROPOSITION 4.5. *Under the assumptions*

$$X_d \ll \ell, \qquad \Omega_d \ll \tau_c^{-1}, \tag{4.28}$$

the variance of CINT at its peak, $\vec{\boldsymbol{y}}^S = \vec{\boldsymbol{y}}$, is given by

$$\mathrm{Var}\left[\mathcal{I}^{CINT}(\vec{\boldsymbol{y}})\right] \approx \frac{1}{2}\left(\frac{\tau_c^2}{\tau_c^2+\frac{1}{\Omega_d^2}+\frac{1}{2B^2}}\right)^2 \left[\frac{1}{a^{2n}}\int_{\mathcal{A}} d\boldsymbol{x}\int_{\mathcal{A}} d\boldsymbol{x}'\,\mathcal{C}^2\left(\frac{|\boldsymbol{x}-\boldsymbol{x}'|}{\ell}\right)\right]\left|\mathbb{E}\left[\mathcal{I}^{CINT}(\vec{\boldsymbol{y}})\right]\right|^2. \tag{4.29}$$

Therefore, the SNR is

$$SNR^{CINT} = \frac{|\mathbb{E}\{\mathcal{I}^{CINT}(\vec{\boldsymbol{y}})\}|}{\sqrt{Var\{\mathcal{I}^{CINT}(\vec{\boldsymbol{y}})\}}} \approx \frac{\sqrt{2}\left(\tau_c^2 + \frac{1}{\Omega_d^2} + \frac{1}{2B^2}\right)}{\tau_c^2 C_{\mathcal{A},\ell}}, \tag{4.30}$$

where

$$C_{\mathcal{A},\ell}^2 = \frac{1}{a^{2n}} \int_{\mathcal{A}} d\boldsymbol{x} \int_{\mathcal{A}} d\boldsymbol{x}'\, \mathcal{C}^2\left(\frac{|\boldsymbol{x}-\boldsymbol{x}'|}{\ell}\right). \tag{4.31}$$

The first assumption in (4.28) holds when $X_d \lesssim X_c$, because $X_c \ll \ell$ by definition (3.20). We explain in the following section that the choice $X_d \sim X_c$ is optimal from the point of view of focusing, and that when $X_d \gg X_c$, it plays no role in $\mathbb{E}\{\mathcal{I}^{\text{CINT}}(\vec{\boldsymbol{y}}^S)\}$. We can assume therefore that $X_d \lesssim X_c \ll \ell$. Similarly, if $\Omega_d \gg \tau_c^{-1}$, it plays no role in $\mathbb{E}\{\mathcal{I}^{\text{CINT}}(\vec{\boldsymbol{y}}^S)\}$. The frequency threshold should satisfy $\Omega_d \lesssim \tau_c^{-1}$. We assume that it is much smaller in (4.28) to simplify the variance calculation, as explained in Appendix E. If $\Omega_d \sim \tau_c^{-1}$, one can show that the same result holds in the narrow band case $B \ll \tau_c^{-1}$.

4.4.4. Comparison between the KM and CINT imaging functions. Let us look at the similarities and differences between the CINT mean point spread function (4.27) and the mean KM point spread function (4.18). They both peak at the source location $\vec{\boldsymbol{y}}$, where the search point offsets $\boldsymbol{\xi}$ and η vanish, but they have different resolution.

The range resolution of $\mathbb{E}\{\mathcal{I}^{\text{CINT}}\}$ is

$$|\eta| \lesssim \frac{c_o}{B}\sqrt{1 + 2B^2\tau_c^2 + \frac{2B^2}{\Omega_d^2}}, \tag{4.32}$$

and it is worse than that of KM, given by (4.17). If we choose the thresholding frequency as $\Omega_d \gg \Omega_c = \tau_c^{-1}$, then it plays no role in $\mathbb{E}\{\mathcal{I}^{\text{CINT}}\}$. If we choose $\Omega_d \ll \tau_c^{-1}$, then the range resolution is much worse than that of KM. Thus, from the point of view of focusing, the choice $\Omega_d \sim \tau_c^{-1}$ is optimal, as it gives a comparable range resolution to that of KM. If $B\tau_c \lesssim 1$, this range resolution is comparable to that in homogeneous media. It is worse when τ_c is so large that $B\tau_c \gg 1$. Then, we have

$$|\eta| \lesssim \frac{c_o}{\Omega_c} = c_o\tau_c. \tag{4.33}$$

This is the CINT range resolution obtained in [11, 9, 10], with a more complicated model based on the forward scattering or parabolic approximation in random media.

The cross-range resolution of $\mathbb{E}\{\mathcal{I}^{\text{CINT}}\}$ is

$$|\boldsymbol{\xi}| \lesssim \frac{\lambda_o L}{a}\sqrt{\frac{a^2}{X_d^2} + \frac{a^2}{X_c^2}}, \tag{4.34}$$

and it is worse than that of KM. If we choose $X_d \gg X_c$, the sensor offset threshold X_d plays no role in $\mathbb{E}\{\mathcal{I}^{\text{CINT}}\}$, and if $X_d \ll X_c$, the cross-range resolution deteriorates significantly. Thus, we see as above, that the optimal choice from the point of view of focusing is $X_d \sim X_c$, and the cross-range resolution becomes

$$|\boldsymbol{\xi}| \lesssim \frac{\lambda_o L}{X_c}, \tag{4.35}$$

with the role of the aperture replaced by the decoherence length X_c. This is the CINT cross-range resolution obtained in [11, 9, 10].

The fluctuations of the the peak values of CINT and KM are very different. While $\mathbb{E}\{\mathcal{I}^{\rm KM}(\vec{\boldsymbol{y}})\}$ is exponentially damped as $e^{-\omega_o^2\tau_c^2}$, the decay of $\mathbb{E}\{\mathcal{I}^{\rm CINT}(\vec{\boldsymbol{y}})\}$ is only polynomial in $\omega_o\tau_c$. More importantly, the SNR of the two imaging functions at $\vec{\boldsymbol{y}}$ is very different. The SNR of KM is given by (4.20) and it decays exponentially with $(\omega_o\tau_c)^2$, no matter how large the aperture a is. This means that KM is not useful for imaging in regimes with large wave front distortions, $\omega_o\tau_c \gg 1$, because the fluctuations of the image caused by the random medium are large and we cannot expect to observe the peak of $\mathcal{I}^{\rm KM}(\vec{\boldsymbol{y}}^S)$ at the true location $\vec{\boldsymbol{y}}$. The peak of the image function dances around the unknown $\vec{\boldsymbol{y}}$ in an unpredictable manner, as illustrated with numerical simulations in section 6.

The SNR of the CINT imaging function at $\vec{\boldsymbol{y}}$ is given by equation (4.30). As τ_c grows (recall (3.14)), the SNR becomes independent of τ_c when $\Omega_d \sim \tau_c^{-1}$. The SNR increases as $(\Omega_d\tau_c)^{-2}$ when $\Omega_d \ll \tau_c^{-1}$. It is not surprising that increasing the bandwidth B does not improve the SNR. This is because the random travel time model accounts only for wave front distortion and does not take into consideration delay spread. However, the array aperture plays a significant role. The larger the aperture, the larger the SNR. In fact, the SNR becomes larger than one for $\ell \lesssim a$. Therefore, the CINT imaging function gives a reliable estimate of the unknown source location $\vec{\boldsymbol{y}}$, even in regimes with large wave front distortions, where KM is not useful. The fluctuations of the CINT imaging function are small and the mean point spread function is a good approximation of $\mathcal{I}^{\rm CINT}(\vec{\boldsymbol{y}}^S)$ for $\vec{\boldsymbol{y}}^S$ in the vicinity of $\vec{\boldsymbol{y}}$.

4.4.5. Resolution versus statistical stability in CINT. Now that we have analyzed in detail the effect of the thresholding parameters Ω_d and X_d on the CINT imaging function, we can discuss the trade-off between its resolution and stability. Mathematically, we may express the trade-off as the following optimization problem: Minimize with respect to Ω_d and X_d the function

$$\frac{V^{\rm CINT}}{V_o} + \frac{1}{{\rm SNR}^{\rm CINT}}.$$

Here

$$V^{\rm CINT} = \frac{\int d\vec{\boldsymbol{y}}^S \mathbb{E}\left[\mathcal{I}^{\rm CINT}(\vec{\boldsymbol{y}}^S)\right]}{\mathbb{E}\left[\mathcal{I}^{\rm CINT}(\vec{\boldsymbol{y}})\right]} \quad \text{and} \quad V_o = \frac{\int d\vec{\boldsymbol{y}}^S \mathbb{E}\left[\left|\mathcal{I}_o^{\rm KM}(\vec{\boldsymbol{y}}^S)\right|^2\right]}{\mathbb{E}\left[\left|\mathcal{I}_o^{\rm KM}(\vec{\boldsymbol{y}})\right|^2\right]} \tag{4.36}$$

quantify the spatial spread of $\mathcal{I}^{\rm CINT}$ in the random medium and in the homogeneous medium, respectively. Recall that when $\Omega_d, X_d \to \infty$, the CINT imaging function becomes the square of the KM function. With the previous results we find that, up to a multiplicative order one constant, we have

$$\frac{V^{\rm CINT}}{V_o} + \frac{1}{{\rm SNR}^{\rm CINT}} \sim \Big(\frac{X_c^2}{X_d^2}\Big)^{\frac{d}{2}} \Big(\frac{1}{\Omega_d^2\tau_c^2}\Big)^{\frac{1}{2}} + C_{\mathcal{A},\ell}\Omega_d^2\tau_c^2. \tag{4.37}$$

This is assuming $\Omega_d \lesssim B$, and it suggests taking $X_d \simeq X_c$ and $\Omega_d \simeq \tau_c^{-1}$, to obtain an SNR of the order of $1/C_{\mathcal{A},\ell}$. If $C_{\mathcal{A},\ell} \ll 1$, then the SNR is much larger than one which means a statistically stable image. This occurs for large aperture arrays. If the aperture is small, so that $C_{A,\ell} \lesssim 1$, we should take a smaller Ω_d to ensure the statistical stablity.

Thus, the thresholding parameters $X_d \simeq X_c$ and $\Omega_d \simeq \tau_c^{-1}$ achieve a good trade-off between resolution and stability, if the array is large enough. When taking smaller frequency thresholds $\Omega_d \ll \tau_c^{-1}$, we increase

the SNR but we also reduce the range resolution. The SNR is not affected by X_d, but the cross-range resolution is. Thus, we should take $X_d \approx X_c$. In practice, these parameters are difficult to estimate directly from the data, so it is better to determine them adaptively, by optimizing over Ω_d and X_d the quality of the resulting image. This is exactly what is done in adaptive CINT [9].

5. Imaging with active arrays. We assume the same set of hypotheses as in the case of passive array, but now $\vec{\boldsymbol{y}}$ is the location of a point reflector. We consider first, in section 5.1, the mean KM point spread function. We show that it peaks at the reflector location $\vec{\boldsymbol{y}}$, but it is exponentially damped by the random medium, just as in the passive array case studied in section 4.3. It can also be shown, after a lengthy calculation that is not included here, that similar to what is stated in Proposition 4.1, the variance of the KM function at $\vec{\boldsymbol{y}}$ does not decay. Therefore, the SNR of the KM point spread function is exponentially small, and the method is statistically unstable. The study of CINT with active arrays is in section 5.2. We obtain first the representation of CINT as the smoothed Wigner transform. Then, we discuss its peak and its statistical stability.

The data model is

$$\widehat{p}(\omega, \vec{\boldsymbol{x}}_r, \vec{\boldsymbol{x}}_s) \approx \widehat{f}(\omega)\alpha_o^2(L,\omega)e^{i\omega[\tau_o(\vec{\boldsymbol{x}}_r,\vec{\boldsymbol{y}})+\tau_o(\vec{\boldsymbol{x}}_s,\vec{\boldsymbol{y}})]+i\omega[\nu(\boldsymbol{x}_r)+\nu(\boldsymbol{x}_s)]}. \tag{5.1}$$

It follows from (2.7), the random travel time model (3.10) and the same approximations of the background Green's function as in section 4.2.

5.1. Kirchhoff migration imaging. The KM point spread function is given by (2.8):

$$\mathcal{I}^{\rm KM}(\vec{\boldsymbol{y}}^S) \approx \alpha_o^2(L,\omega_o)\int_{\mathcal{A}} d\boldsymbol{x}_s \int_{\mathcal{A}} d\boldsymbol{x}_r \int_{-\infty}^{\infty} \frac{d\omega}{2\pi}\widehat{f}(\omega)\, e^{-2i\frac{\omega\eta}{c_o}+i\frac{\omega_o}{c_o}\frac{(\boldsymbol{x}_r+\boldsymbol{x}_s)\cdot\boldsymbol{\xi}}{L}+i\omega[\nu(\boldsymbol{x}_s)+\nu(\boldsymbol{x}_r)]}, \tag{5.2}$$

where we used the random travel time model (4.8) and approximations (4.4) and (4.6) of the travel times. Given the moment formula (3.18) with $\omega' = -\omega$, and changing variables to $\boldsymbol{x} = \frac{\boldsymbol{x}_r+\boldsymbol{x}_s}{2}$, $\widetilde{\boldsymbol{x}} = \boldsymbol{x}_r - \boldsymbol{x}_s$, we obtain

$$\mathbb{E}\left\{\mathcal{I}^{\rm KM}(\vec{\boldsymbol{y}}^S)\right\} \approx \alpha_o^2(L,\omega_o)\int_{\mathcal{A}} d\boldsymbol{x}\, e^{2i\frac{\omega_o}{c_o}\frac{\boldsymbol{x}\cdot\boldsymbol{\xi}}{L}} \int_{S(\boldsymbol{x})} d\widetilde{\boldsymbol{x}} \int_{-\infty}^{\infty} \frac{d\omega}{2\pi}\widehat{f}(\omega)\, e^{-2i\frac{\omega\eta}{c_o}-\omega^2\tau_c^2[1+\mathcal{C}(|\widetilde{\boldsymbol{x}}|/\ell)]}, \tag{5.3}$$

where $S(\boldsymbol{x})$, $\boldsymbol{x}\in\mathcal{A}$, is the set of points $\widetilde{\boldsymbol{x}}$ defined by

$$S(\boldsymbol{x}) = \left\{\widetilde{\boldsymbol{x}}\in\mathbb{R}^n \text{ s.t. } \boldsymbol{x}\pm\frac{\widetilde{\boldsymbol{x}}}{2}\in\mathcal{A}\right\}.$$

The mean point spread function follows from (5.3), after substituting the Gaussian pulse (2.3) and integrating over the bandwidth

$$\begin{aligned}\mathbb{E}\left\{\mathcal{I}^{\rm KM}(\vec{\boldsymbol{y}}^S)\right\} \approx \alpha_o^2(L,\omega_o)\int_{\mathcal{A}} d\boldsymbol{x}\, e^{2i\frac{\omega_o}{c_o}\frac{\boldsymbol{x}\cdot\boldsymbol{\xi}}{L}} \int_{S(\boldsymbol{x})} d\widetilde{\boldsymbol{x}}\, \frac{\exp\left\{-\omega_o^2\tau_c^2\frac{[1+\mathcal{C}(|\widetilde{\boldsymbol{x}}|/\ell)]}{\{1+2B^2\tau_c^2[1+\mathcal{C}(|\widetilde{\boldsymbol{x}}|/\ell)]\}}\right\}}{\sqrt{1+2B^2\tau_c^2\left[1+\mathcal{C}(|\widetilde{\boldsymbol{x}}|/\ell)\right]}} \\ \times\exp\left\{-i\frac{\omega_o}{c_o}\frac{2\eta}{\{1+2B^2\tau_c^2\left[1+\mathcal{C}(|\widetilde{\boldsymbol{x}}|/\ell)\right]\}} - \frac{2B^2\eta^2}{c_o^2\{1+2B^2\tau_c^2\left[1+\mathcal{C}(|\widetilde{\boldsymbol{x}}|/\ell)\right]\}}\right\}.\end{aligned} \tag{5.4}$$

It has a complicated expression, but we can clearly infer from it that its maximum is at $\vec{\boldsymbol{y}}$, where the search point offsets $\boldsymbol{\xi}$ and η vanish.

The cross-range resolution of (5.4) is similar to that of images with passive arrays

$$|\boldsymbol{\xi}| \lesssim \frac{\lambda_o 2L}{a}, \tag{5.5}$$

except that we have the round trip distance $2L$ from the array to the reflector. Each source receiver offset $\widetilde{\boldsymbol{x}}$ gives a slightly different range resolution

$$|\eta| \lesssim \frac{c_o}{2B}\sqrt{1+2\gamma B^2\tau_c^2}, \tag{5.6}$$

with $\gamma \in [1,2]$, the interval of values of $1+\mathcal{C}(|\widetilde{\boldsymbol{x}}|/\ell)$. The range resolution is of order $c_o\tau_c$ when $B\tau_c \gg 1$, as in source localization with passive arrays.

The dramatic effect of the random medium on the KM point spread function is the exponential damping factor

$$D = \frac{\exp\left\{-\omega_o^2\tau_c^2 \frac{[1+\mathcal{C}(|\widetilde{\boldsymbol{x}}|/\ell)]}{\{1+2B^2\tau_c^2[1+\mathcal{C}(|\widetilde{\boldsymbol{x}}|/\ell)]\}}\right\}}{\sqrt{1+2B^2\tau_c^2\left[1+\mathcal{C}(|\widetilde{\boldsymbol{x}}|/\ell)\right]}}. \tag{5.7}$$

It implies that the KM image is essentially incoherent, with its random fluctuations dominating the mean, as we have seen in section 4.3 for imaging with passive arrays.

5.2. Coherent interferometric imaging. The CINT imaging function is given by (2.9):

$$\mathcal{I}^{\rm CINT}(\vec{\boldsymbol{y}}^S) = \int_{\mathcal{A}} d\boldsymbol{x}_r \int_{\mathcal{A}} d\boldsymbol{x}_r' \Psi\left(\frac{\boldsymbol{x}_r-\boldsymbol{x}_r'}{X_d}\right) \int_{\mathcal{A}} d\boldsymbol{x}_s \int_{\mathcal{A}} d\boldsymbol{x}_s' \Psi\left(\frac{|\boldsymbol{x}_s-\boldsymbol{x}_s'|}{X_d}\right) \int_{-\infty}^{\infty}\frac{d\omega}{2\pi}\int_{-\infty}^{\infty}\frac{d\omega'}{2\pi}\widehat{\Phi}\left(\frac{\omega-\omega'}{\Omega_d}\right)$$
$$\widehat{p}(\omega,\vec{\boldsymbol{x}}_r,\vec{\boldsymbol{x}}_s)\overline{\widehat{p}(\omega',\vec{\boldsymbol{x}}_r',\vec{\boldsymbol{x}}_s')}\exp\left\{-i\omega\left[\tau_o(\vec{\boldsymbol{x}}_r,\vec{\boldsymbol{y}}^S)+\tau_o(\vec{\boldsymbol{x}}_s,\vec{\boldsymbol{y}}^S)\right]+i\omega'\left[\tau_o(\vec{\boldsymbol{x}}_r',\vec{\boldsymbol{y}}^S)+\tau_o(\vec{\boldsymbol{x}}_s',\vec{\boldsymbol{y}}^S)\right]\right\}. \tag{5.8}$$

We recall the data model (5.1) and rewrite (5.8) in terms of the Wigner transform

$$\mathcal{W}(\omega,\boldsymbol{x};\boldsymbol{\kappa},T) = \int_{\mathbb{R}^n} d\widetilde{\boldsymbol{x}} \int_{-\infty}^{\infty} d\widetilde{\omega}\, \widehat{\mathcal{P}}\left(\omega+\frac{\widetilde{\omega}}{2},\boldsymbol{x}+\frac{\widetilde{\boldsymbol{x}}}{2}\right)\overline{\widehat{\mathcal{P}}\left(\omega-\frac{\widetilde{\omega}}{2},\boldsymbol{x}-\frac{\widetilde{\boldsymbol{x}}}{2}\right)}e^{i\boldsymbol{\kappa}\cdot\widetilde{\boldsymbol{x}}-i\widetilde{\omega}T}. \tag{5.9}$$

Here

$$\mathcal{P}(\omega,\boldsymbol{x}) := \sqrt{\widehat{f}(\omega)}\alpha_o(L,\omega_o)e^{i\omega\tau_o(\vec{\boldsymbol{x}},\vec{\boldsymbol{y}})+i\omega\nu(\boldsymbol{x})} \approx \sqrt{\widehat{f}(\omega)}\widehat{G}(\omega,\vec{\boldsymbol{x}},\vec{\boldsymbol{y}}) \tag{5.10}$$

is almost the same as (4.7), except for the square root of the pulse. We obtain the following result, proved in Appendix F.

PROPOSITION 5.1. *Assume that the thresholding parameters X_d and Ω_d satisfy (4.23). Then, the CINT imaging function is given by the product of two Wigner transforms, smoothed over all the arguments*

$$\mathcal{I}^{CINT}(\vec{\boldsymbol{y}}^S) \approx \frac{\Omega_d X_d^{2n}}{(2\pi)^{n+7/2}}\int_{\mathcal{A}} d\boldsymbol{x}_r \int_{\mathcal{A}} d\boldsymbol{x}_s \int_{-\infty}^{\infty} d\omega \int_{\mathbb{R}^n} d\boldsymbol{\kappa}_r \int_{-\infty}^{\infty} dT_r\, \mathcal{W}(\omega,\boldsymbol{x}_r;\boldsymbol{\kappa}_r,T_r)\int_{\mathbb{R}^n} d\boldsymbol{\kappa}_s \int_{-\infty}^{\infty} dT_s\, \mathcal{W}(\omega,\boldsymbol{x}_s;\boldsymbol{\kappa}_s,T_s)$$
$$\times exp\left\{-\frac{X_d^2\left|\boldsymbol{\kappa}_r-\frac{\omega_o}{c_o}\frac{(\boldsymbol{\xi}-\boldsymbol{x}_r)}{L}\right|^2}{2}-\frac{X_d^2\left|\boldsymbol{\kappa}_s-\frac{\omega_o}{c_o}\frac{(\boldsymbol{\xi}-\boldsymbol{x}_s)}{L}\right|^2}{2}-\frac{\Omega_d^2}{2}\left[T_r+T_s-\tau_o(\vec{\boldsymbol{x}}_r,\vec{\boldsymbol{y}}^S)-\tau_o(\vec{\boldsymbol{x}}_s,\vec{\boldsymbol{y}}^S)\right]^2\right\}. \tag{5.11}$$

To gain insight into the meaning of this result, we study next the Wigner transform under the assumption that the random function μ that models the wave speed fluctuations is smooth. This is the case in particuler when μ has Gaussian statistics with Gaussian covariance function (3.4) [1].

5.2.1. The Wigner transform. We have by definitions (5.9-5.10) that

$$\mathcal{W}(\omega,\boldsymbol{x};\boldsymbol{\kappa},T)\approx\widehat{f}(\omega)|\alpha_o(L,\omega_o)|^2\int_{\mathbb{R}^n}d\widetilde{\boldsymbol{x}}\exp\left\{i\widetilde{\boldsymbol{x}}\cdot\boldsymbol{\kappa}+i\omega\Delta\tau_o(\boldsymbol{x},\widetilde{\boldsymbol{x}})+i\omega\Delta\nu(\boldsymbol{x},\widetilde{\boldsymbol{x}})\right\}$$
$$\times\int_{-\infty}^{\infty}d\widetilde{\omega}\exp\left\{-\frac{\widetilde{\omega}^2}{8B^2}+i\widetilde{\omega}\left[\langle\tau_o\rangle\left(\boldsymbol{x},\widetilde{\boldsymbol{x}}\right)+\langle\nu\rangle(\boldsymbol{x},\widetilde{\boldsymbol{x}})-T\right]\right\}.$$

Here we used the Gaussian expression (2.3) of the pulse and introduced the random functions

$$\Delta\nu(\boldsymbol{x},\widetilde{\boldsymbol{x}})=\nu\left(\boldsymbol{x}+\frac{\widetilde{\boldsymbol{x}}}{2}\right)-\nu\left(\boldsymbol{x}-\frac{\widetilde{\boldsymbol{x}}}{2}\right),\quad\langle\nu\rangle(\boldsymbol{x},\widetilde{\boldsymbol{x}})=\frac{1}{2}\left[\nu\left(\boldsymbol{x}+\frac{\widetilde{\boldsymbol{x}}}{2}\right)+\nu\left(\boldsymbol{x}-\frac{\widetilde{\boldsymbol{x}}}{2}\right)\right].$$

We also let (with $\vec{\boldsymbol{x}}=(\boldsymbol{x},0)$)

$$\Delta\tau_o(\boldsymbol{x},\widetilde{\boldsymbol{x}})=\tau_o\left(\vec{\boldsymbol{x}}+\frac{(\widetilde{\boldsymbol{x}},0)}{2},\vec{\boldsymbol{y}}^S\right)-\tau_o\left(\vec{\boldsymbol{x}}-\frac{(\widetilde{\boldsymbol{x}},0)}{2},\vec{\boldsymbol{y}}^S\right),$$
$$\langle\tau_o\rangle\left(\boldsymbol{x},\widetilde{\boldsymbol{x}}\right)=\frac{1}{2}\left[\tau_o\left(\vec{\boldsymbol{x}}+\frac{(\widetilde{\boldsymbol{x}},0)}{2},\vec{\boldsymbol{y}}^S\right)+\tau_o\left(\vec{\boldsymbol{x}}-\frac{(\widetilde{\boldsymbol{x}},0)}{2},\vec{\boldsymbol{y}}^S\right)\right].$$

Integrating over $\widetilde{\omega}$, we obtain the following expression of the Wigner transform

$$\mathcal{W}(\omega,\boldsymbol{x};\boldsymbol{\kappa},T)\approx2\sqrt{2\pi}B\widehat{f}(\omega)|\alpha_o(L,\omega_o)|^2\int d\widetilde{\boldsymbol{x}}\exp\left\{i\widetilde{\boldsymbol{x}}\cdot\boldsymbol{\kappa}+i\omega\Delta\tau_o(\boldsymbol{x},\widetilde{\boldsymbol{x}})+i\omega\Delta\nu(\boldsymbol{x},\widetilde{\boldsymbol{x}})\right\}$$
$$\exp\left\{-2B^2\left[\langle\tau_o\rangle\left(\boldsymbol{x},\widetilde{\boldsymbol{x}}\right)+\langle\nu\rangle(\boldsymbol{x},\widetilde{\boldsymbol{x}})-T\right]^2\right\}.\qquad(5.12)$$

Next, we use the assumed smoothness of the random medium fluctuations to expand in $\widetilde{\boldsymbol{x}}$. We cannot do it directly in (5.12), because the $\widetilde{\boldsymbol{x}}$ integral extends to the whole $\mathbb{R}^n$. However, we can expand in the Wigner transform smoothed over directions

$$\int_{\mathbb{R}^n}d\boldsymbol{\kappa}\,\mathcal{W}(\omega,\boldsymbol{x};\boldsymbol{\kappa},T)e^{-\frac{X_d^2}{2}\left|\boldsymbol{\kappa}-\frac{\omega_o}{c_o}\frac{(\boldsymbol{\xi}-\boldsymbol{x})}{L}\right|^2}=\frac{2(2\pi)^{(n+1)/2}B}{X_d^n}\widehat{f}(\omega)|\alpha_o(L,\omega_o)|^2\int d\widetilde{\boldsymbol{x}}\,e^{-\frac{|\widetilde{\boldsymbol{x}}|^2}{2X_d^2}}$$
$$\times\exp\left\{i\frac{\omega_o}{c_o}\frac{\widetilde{\boldsymbol{x}}\cdot\boldsymbol{\xi}}{L}+i\omega\Delta\nu(\boldsymbol{x},\widetilde{\boldsymbol{x}})-2B^2\left[\tau_o(\vec{\boldsymbol{x}},\vec{\boldsymbol{y}})+\langle\nu\rangle(\boldsymbol{x},\widetilde{\boldsymbol{x}})-T\right]^2\right\},\qquad(5.13)$$

where $|\widetilde{\boldsymbol{x}}|$ is restricted by the standard deviation X_d of the Gaussian. Here we used approximation (4.4) of the travel time to calculate $\Delta\tau_o(\boldsymbol{x},\widetilde{\boldsymbol{x}})$ and $\langle\tau_o\rangle\left(\boldsymbol{x},\widetilde{\boldsymbol{x}}\right)$.

We make the following simplifying assumptions on the thresholding parameters and the strength σ of the fluctuations, in order to linearize the phase in (5.13)

$$\frac{\sigma L}{\lambda_o}\left(\frac{X_d}{\ell}\right)^3\ll1,\qquad\frac{B}{\omega_o}\frac{\sigma L}{\lambda_o}\left(\frac{X_d}{\ell}\right)^2\ll1,\qquad\frac{B}{\omega_o}\frac{\sigma L}{\lambda_o}\frac{X_d}{\ell}\ll1.\qquad(5.14)$$

Since $B\ll\omega_o$, this holds for example when

$$\frac{\sigma L}{\lambda_o}\lesssim1,\qquad X_d\ll\ell,\quad\text{or when}\quad\frac{\sigma L}{\lambda_o}\ll1,\qquad X_d\lesssim\ell.$$

In particular, if $X_d\sim X_c$, then $X_d\ll\ell$ by (3.20). With the assumptions (5.14), we can write

$$\omega\Delta\nu(\boldsymbol{x},\widetilde{\boldsymbol{x}})==\omega_o\widetilde{\boldsymbol{x}}\cdot\nabla_{\boldsymbol{x}}\nu(\boldsymbol{x})+O\left[\frac{B}{\omega_o}\frac{\sigma L}{\lambda_o}\frac{X_d}{\ell}\right]+O\left[\frac{\sigma L}{\lambda_o}\left(\frac{X_d}{\ell}\right)^3\right]\approx\omega_o\widetilde{\boldsymbol{x}}\cdot\nabla_{\boldsymbol{x}}\nu(\boldsymbol{x}),\qquad(5.15)$$

and

$$B\langle\nu\rangle(\boldsymbol{x},\widetilde{\boldsymbol{x}}) = B\nu(\boldsymbol{x}) + O\left[\frac{B}{\omega_o}\frac{\sigma L}{\lambda_o}\left(\frac{X_d}{\ell}\right)^2\right] \approx B\nu(\boldsymbol{x}), \tag{5.16}$$

and we obtain from (5.13), after evaluating the $\widetilde{\boldsymbol{x}}$ integral, the following result.

PROPOSITION 5.2. *Under the assumptions (5.14), the Wigner transform smoothed over directions is given by*

$$\int_{\mathbb{R}^n} d\boldsymbol{\kappa}\, \mathcal{W}(\omega,\boldsymbol{x};\boldsymbol{\kappa},T) e^{-\frac{X_d^2}{2}\left|\boldsymbol{\kappa}-\frac{\omega_o}{c_o}\frac{(\boldsymbol{\xi}-\boldsymbol{x})}{L}\right|^2} \approx (2\pi)^{n+1}|\alpha_o(L,\omega_o)|^2 e^{-\frac{(\omega-\omega_o)^2}{2B^2}} \mathcal{F}(\boldsymbol{x},T,\boldsymbol{\xi}), \tag{5.17}$$

with random

$$\mathcal{F}(\boldsymbol{x},T,\boldsymbol{\xi}) = exp\left\{-2\pi^2\left(\frac{X_d}{\lambda_o}\right)^2 |\boldsymbol{\xi}/L + c_o\nabla_{\boldsymbol{x}}\nu(\vec{\boldsymbol{x}})|^2 - 2B^2\left[\tau_o(\vec{\boldsymbol{x}},\vec{\boldsymbol{y}}) + \nu(\boldsymbol{x}) - T\right]^2\right\} \tag{5.18}$$

peaking at $\boldsymbol{\xi} = -c_o L\nabla_{\boldsymbol{x}}\nu(\boldsymbol{x})$ *and* $T = \tau_o(\vec{\boldsymbol{x}},\vec{\boldsymbol{y}}) + \nu(\boldsymbol{x})$.

Note that if the fluctuations are stronger, so that the first assumption in (5.14) does not hold, but the other two do, due to the fact that $B \ll \omega_o$, we can still write an equation like (5.17), except that the $\widetilde{\boldsymbol{x}}$ integral is more difficult to evaluate, because it involves a cubic phase in $\widetilde{\boldsymbol{x}}$. Nevertheless, the conclusions about the stability of CINT, drawn below, hold.

5.2.2. The CINT point spread function. Gathering our results, we obtain that the CINT point function described in Proposition 5.1 is given by

$$\begin{aligned}\mathcal{I}^{\text{CINT}}(\vec{\boldsymbol{y}}^S) \approx (2\pi)^{n-\frac{3}{2}}|\alpha_o(L,\omega_o)|^4\Omega_d X_d^{2n}\int_{-\infty}^{\infty} e^{-\frac{(\omega-\omega_o)^2}{B^2}}\int_{\mathcal{A}} d\boldsymbol{x}_r\int_{-\infty}^{\infty} dT_r\,\mathcal{F}(\boldsymbol{x}_r,T_r,\boldsymbol{\xi})\\ \times\int_{\mathcal{A}} d\boldsymbol{x}_s\int_{-\infty}^{\infty} dT_s\,\mathcal{F}(\boldsymbol{x}_s,T_s,\boldsymbol{\xi})\exp\left\{-\frac{\Omega_d^2}{2}\left[T_r+T_s-\tau_o(\vec{\boldsymbol{x}}_r,\vec{\boldsymbol{y}}^S)-\tau_o(\vec{\boldsymbol{x}}_s,\vec{\boldsymbol{y}}^S)\right]^2\right\}.\end{aligned} \tag{5.19}$$

It is the product of the random function $\mathcal{F}(\boldsymbol{x},T,\boldsymbol{\xi})$ smoothed by integration over the aperture and by convolution in time with a time window of support $|T| \lesssim 1/\Omega_d$. The integral over the bandwidth plays no role in the smoothing within the context of the random travel time model. This is consistent with the results in sections 4.4.3-4.4.4, which say that in our regime we cannot improve the statistical stability of $\mathcal{I}^{\text{CINT}}$ by simply increasing the bandwidth as far as wave distortion effects alone are concerned.

We rewrite (5.19) in more explicit form, by substituting the expression (5.18) and carrying out the T_r and T_s integrals. We obtain

$$\begin{aligned}\mathcal{I}^{\text{CINT}}(\vec{\boldsymbol{y}}^S) \approx \frac{\pi^2(2\pi)^{n-2}|\alpha_o(L,\omega_o)|^4\Omega_d X_d^{2n}}{\sqrt{2(\Omega_d^2+2B^2)}}\int_{\mathcal{A}} d\boldsymbol{x}_r\int_{\mathcal{A}} d\boldsymbol{x}_s\exp\left\{-\frac{\Omega_d^2B^2\left[\Delta T(\boldsymbol{x}_r)+\Delta T(\boldsymbol{x}_s)\right]^2}{\Omega_d^2+2B^2}\right\}\\ \times\exp\left\{-2\pi^2\left(\frac{X_d}{\lambda_o}\right)^2|\boldsymbol{\xi}/L+c_o\nabla_{\boldsymbol{x}}\nu(\boldsymbol{x}_r)|^2 - 2\pi^2\left(\frac{X_d}{\lambda_o}\right)^2|\boldsymbol{\xi}/L+c_o\nabla_{\boldsymbol{x}}\nu(\boldsymbol{x}_s)|^2\right\},\end{aligned} \tag{5.20}$$

where

$$\Delta T(\boldsymbol{x}) = \tau_o(\vec{\boldsymbol{x}},\vec{\boldsymbol{y}}^S) - \tau_o(\vec{\boldsymbol{x}},\vec{\boldsymbol{y}}) - \nu(\boldsymbol{x}), \qquad \vec{\boldsymbol{x}} = (\boldsymbol{x},0). \tag{5.21}$$

Now we can draw an analogy to the results in section 4.4.3, in order to assess the peaking and stability properties of $\mathcal{I}^{\text{CINT}}(\vec{\boldsymbol{y}}^S)$.

After the same calculations as above, the CINT point spread function with passive arrays becomes

$$\begin{aligned}\mathcal{I}^{\rm CINT}_{\rm pas}(\vec{\boldsymbol{y}}^S) &\sim \int_{\mathcal{A}} d\boldsymbol{x}_r \int_{-\infty}^{\infty} dT_r\, \mathcal{F}(\boldsymbol{x}_r, T_r, \boldsymbol{\xi}) \exp\left\{-\frac{\Omega_d^2}{2}\left[T_r - \tau_o(\vec{\boldsymbol{x}}_r, \vec{\boldsymbol{y}}^S)\right]^2\right\} \\ &= \int_{\mathcal{A}} d\boldsymbol{x}_r \int_{-\infty}^{\infty} dT_r \exp\left\{-2\pi^2\left(\frac{X_d}{\lambda_o}\right)^2 |\boldsymbol{\xi}/L + c_o\nabla_{\boldsymbol{x}}\nu(\boldsymbol{x}_r)|^2 - 2B^2\left[\tau_o(\vec{\boldsymbol{x}}_r, \vec{\boldsymbol{y}}) + \nu(\boldsymbol{x}_r) - T_r\right]^2\right\} \\ &\qquad \times \exp\left\{-\frac{\Omega_d^2}{2}\left[T_r - \tau_o(\vec{\boldsymbol{x}}_r, \vec{\boldsymbol{y}}^S)\right]^2\right\}. \end{aligned} \tag{5.22}$$

Here the symbol $\sim$ denotes approximate, up to a multiplicative constant of order one, and the index "pas" reminds us that (5.22) applies to source localization with passive arrays. Moreover, we can carry out the T_r integral and obtain

$$\mathcal{I}^{\rm CINT}_{\rm pas}(\vec{\boldsymbol{y}}^S) \sim \int_{\mathcal{A}} d\boldsymbol{x}_r \exp\left\{-2\pi^2\left(\frac{X_d}{\lambda_o}\right)^2 |\boldsymbol{\xi}/L + c_o\nabla_{\boldsymbol{x}}\nu(\boldsymbol{x}_r)|^2 - \frac{2\Omega_d^2 B^2\left[\Delta T(\boldsymbol{x}_r)\right]^2}{\Omega_d^2 + 4B^2}\right\}. \tag{5.23}$$

Thus, the CINT point spread function (5.20) has a form comparable to the square of (5.23), except for the slightly different coefficient in the ΔT terms and the cross-terms $\Delta T(\boldsymbol{x}_r)\Delta T(\boldsymbol{x}_s)$. These weights make a quantitative but not a qualitative difference, and do not seem to play a significant role in the focusing and stability of $\mathcal{I}^{\rm CINT}(\vec{\boldsymbol{y}}^S)$.

We can now state the main conclusion from the analysis this section which is that if the conditions stated in section 4.4.3 hold, so that CINT with passive arrays has a high SNR, then so will CINT with active arrays. Moreover, the resolution of the two point spread functions will be similar. The statistical stability of CINT (i.e., the high SNR) is due to the smoothing over $\boldsymbol{x}_r$ and $\boldsymbol{x}_s$. For each receiver location, the integrand peaks at the random cross-range

$$\boldsymbol{\xi} = -c_o L \nabla_{\boldsymbol{x}}\nu(\boldsymbol{x}_r). \tag{5.24}$$

and at the random range satisfying

$$\tau_o(\vec{\boldsymbol{x}}_r, \vec{\boldsymbol{y}}^S) = \tau_o(\vec{\boldsymbol{x}}_r, \vec{\boldsymbol{y}}) + \nu(\boldsymbol{x}_r), \quad \text{that is} \quad \eta = c_o\nu(\boldsymbol{x}_r) + O\left(\frac{a|\boldsymbol{\xi}|}{L}\right). \tag{5.25}$$

The integration over the aperture averages these random fluctuations, but it also blurs the image by taking the envelope of the peaks (5.24)-(5.25). A similar smoothing is by integration over $\boldsymbol{x}_s$.

6. Numerical results. We illustrate with numerical simulations the performance of the KM and CINT imaging functions with active arrays. The simulations are in two dimensions, with a linear array of $N = 101$ sensors, distributed uniformly over the cross-range interval $[-2\ell, 2\ell]$. Each sensor emits a pulse $f(t)$, that is a modulated sinc function, with constant Fourier coefficients in the bandwidth $[125, 175]$kHz. The medium is randomly inhomogeneous, with wave speed $c(\vec{\boldsymbol{x}})$ given by (3.1), where $c_o = 3$km/s so that the central wavelength is $\lambda_o = 2$cm. The correlation length is $\ell = 100\lambda_o$ and the standard deviation of the fluctuations is either $\sigma = 0.04\%$ or $\sigma = 0.1\%$. We show a realization of μ in Figure 6.1. The medium contains a small, point-like reflector that we wish to image, at $\vec{\boldsymbol{y}} = (0, L = 99\ell)$.

We compute the array data

$$\widehat{p}(\omega, \vec{\boldsymbol{x}}_r, \vec{\boldsymbol{x}}_s) = \widehat{f}(\omega)\widehat{G}(\omega, \vec{\boldsymbol{x}}_r, \vec{\boldsymbol{y}})\widehat{G}(\omega, \vec{\boldsymbol{x}}_s, \vec{\boldsymbol{y}})$$

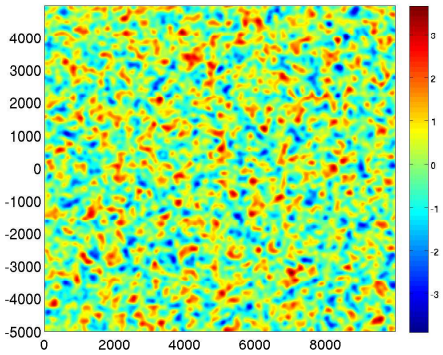

FIG. 6.1. *Left: A realization of the random function μ used in (3.1) to model the wave speed fluctuations. The axes are range and cross-range scaled by λ_o. The colorbar shows the amplitude fluctuations of the dimensionless μ.*

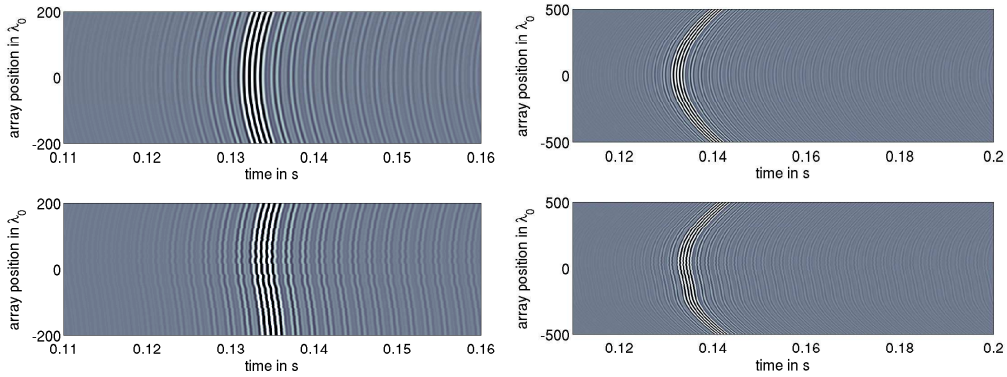

FIG. 6.2. *Top row: The time traces in the homogeneous medium. Bottom row: The time traces in a realization of the random medium, with $\sigma = 0.1\%$. The left column is for the small aperture $[-2\ell, 2\ell]$ used to compute the KM and CINT images. The right column is for the larger aperture $[-5\ell, 5\ell]$. The illumination is from the central element in the array.*

for $\omega \in [125, 175]$kHz, using 100 frequencies to discretize the bandwidth. Here $\widehat{G}(\omega, \vec{\boldsymbol{x}}_r, \vec{\boldsymbol{y}})$ is given by (3.10) with $\nu_\tau(\boldsymbol{x})$ as in (3.11). The integral along the straight rays is computed with numerical quadrature. The wave front distortion can be seen in the traces displayed in Figure 6.2, specially in the case of the larger aperture shown on the right.

a	$\sigma = 4e-4$	$\sigma = 1e-3$
mean(CINT)	0.0019	6.5e-4
std(CINT)	9.87e-4	6.16e-4
SNR(CINT)	1.92	1.06

TABLE 6.1
Mean, std and SNR for CINT at target

In tables 6.1 and 6.2 we give the values of the mean, the standard deviation and the SNR of the KM and CINT imaging functions at their peak. As predicted by the theory, CINT performs very well in clutter while KM is unstable. This is reflected in the values of the SNR which is approximately 100 times larger for CINT. The statistical stability of CINT is obtained at the expense of some loss in resolution, as seen from the blur of the images in the bottom row in Figure 6.4.

We show in Figure 6.3 the mean of the KM and CINT imaging functions, divided by their standard

a	$\sigma = 4e-4$
mean(KM)	0.68
std(KM)	25.79
SNR(KM)	0.0265

TABLE 6.2
Mean, std and SNR for KM at target

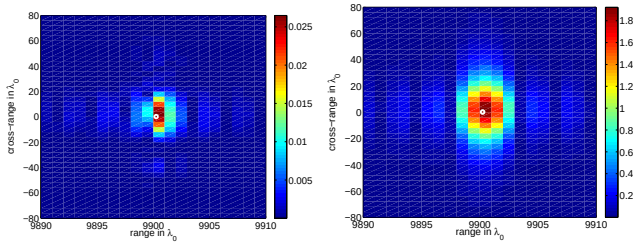

FIG. 6.3. *The mean of the KM and CINT images divided by their standard deviation at the peak. KM is on the left and CINT on the right. As predicted by the theory, the mean of both imaging functions peaks at the true reflector location indicated by a white dot. The colorbar shows that the SNR of CINT is approximately* 100 *times larger than that of KM. The axes are range and cross-range in* λ_o.

deviation at the peak. The mean and standard deviation are estimated from the images computed for many realizations of the random medium. We observe that, as predicted by the theory, the mean of both the KM and CINT images peaks at the true target location indicated in Figure 6.3 with a white dot. The colorbar shows that the SNR of KM is very small, which means that the KM images are not statistically stable. This is illustrated in the top row in Figure 6.4, where we show the KM images in three different realizations of the random medium. Note how the peak dances around the true location of the reflector, indicated with the white dot. The SNR of CINT is approximately 100 times larger than that of KM. This is why the peak of the CINT images, shown in the bottom row in Figure 6.4, is close to the true location of the reflector in all the realizations.

Note that we plot in Figure 6.4 the square root of the CINT image to compare it with KM. The CINT image is equal to the square of the KM image only if there is no thresholding over the frequencies and sensor offsets in the calculation of the cross-correlations of the traces. Here we use the thresholds to get statistical stability, so the CINT images are obviously not the square of the KM ones. Nevertheless, we plot in the bottom row of Figure 6.4 the square root of the CINT images to have a fair comparison with the resolution of the mean KM image, and note the range and cross-range blur predicted by the theory of CINT.

7. Summary. We have presented a comparative analytical study of resolution and statistical stability of two array imaging methods in random media. The first method is the widely used Kirchhoff migration (KM) and the second is coherent interferometry (CINT). It is known that KM is robust with respect to additive noise, such as measurement noise [3, 4]. This is illustrated for example in [12], where it is also shown how KM fails to image in random (cluttered) media. Clutter "noise" in the data and in the images has a complex structure, in which correlations play an important role. By clutter noise in the images we mean their random fluctuations due to fluctuations in the medium properties. We have analyzed the KM and CINT point spread functions for passive and active arrays of sensors, and quantified explicitly their resolution limits and their signal-to-noise ratio (SNR). The SNR is defined as the mean point spread function at its

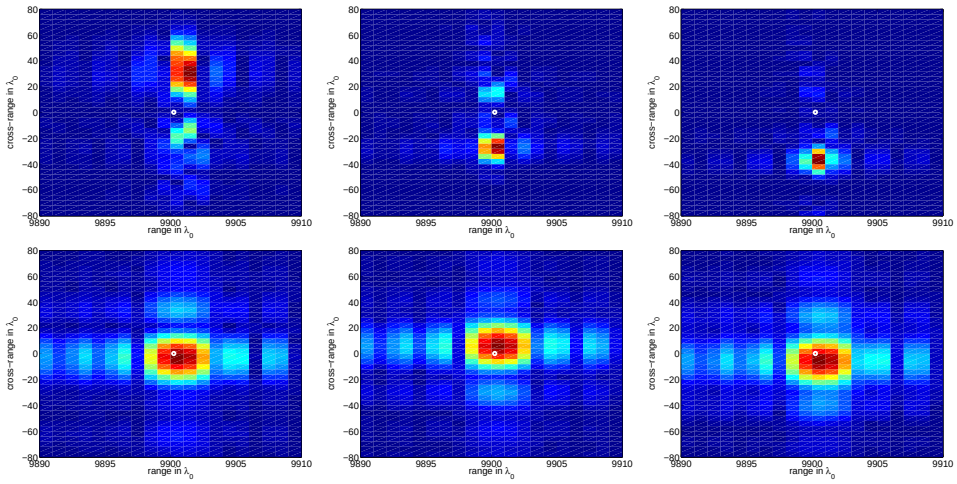

FIG. 6.4. *Top row: KM images in three realizations of the random medium. Note how the peak dances around the true location of the reflector, indicated with the white dot. Bottom row: Square root of the CINT images in the same three realizations of the random medium. Note that the peak is close to the true reflector location in all the realizations, as predicted by the theory. The axes are range and cross-range in* λ_o.

peak divided by its standard deviation.

To carry out analytically the resolution and SNR comparative study of KM and CINT, we have used the relatively simple random travel time model for the medium effects on the array data. The model is valid in the regime of geometrical optics in random media. In this regime wave diffraction, amplitude fluctuations and power delay spread due to multiple scattering are negligible, while wave front distortions are significant and well-captured by the model. CINT and KM in random media have been studied before in [11, 9], using the parabolic approximation model. However, an explicit analytical SNR calculation was not done in [11, 9], because the forward scattering model is too complicated to allow evaluation of higher order statistical moments of the array data. The results in [11, 9] agree qualitatively with those obtained in this paper.

We have focused the analysis on the case of large wave front distortions, where the random medium has a significant effect on the imaging process. The results show that: (1) The KM and CINT imaging functions provide an unbiased estimate of the source or reflector locations. That is to say, the statistical mean of their point spread functions peak at the true location $\vec{\boldsymbol{y}}$ of the sources or reflectors that we wish to image. (2) The SNR of the KM and CINT imaging functions in the vicinity of $\vec{\boldsymbol{y}}$ is dramatically different. The SNR of KM is exponentially small with range, no matter how large the bandwidth or the array aperture is. This means that KM is not statistically stable and it cannot be used for imaging in regimes with large wave front distortions. The random fluctuations of the images are large and we cannot expect to observe the peak of the images near $\vec{\boldsymbol{y}}$. The peaks dance around $\vec{\boldsymbol{y}}$ in an unpredictable manner. The CINT imaging method is clearly superior to KM because its SNR is not small and it is enhanced by increasing the aperture. However, the statistical stability of CINT comes at the expense of some blurring of the images. We have quantified explicitly the trade-off between the resolution and stability of the CINT imaging function. We have also illustrated the theoretical results with some numerical simulations.

Acknowledgments. The work of L. Borcea was partially supported by the Office of Naval Research, grant N00014-09-1-0290, and by the National Science Foundation, grants DMS-0907746 and DMS-0934594.

J. Garnier and G. Papanicolaou thank the Institut des Hautes Études Scientifiques (IHÉS) for its hospitality while this work was completed. The work of G. Papanicolaou was partially supported by AFOSR grant FA9550-08-1-0089. The work of C. Tsogka was partially supported by the European Research Council Stanting Grant, GA 239959.

Appendix A. Domain of validity of the random travel time model. Within the geometric optics approximation, the amplitude and phase perturbations of the wave are given in [21, 19] in terms of the fluctuations of the index of refraction along the path of propagation. In this appendix we derive for consistency these equations (see (A.1-A.2)) and we study under which conditions the random travel time model is valid (see (A.7)).

In the geometric optics approximation, the wave has the form $u = \alpha e^{i\omega\tau}$, where α is the amplitude and τ is the travel time. The travel time is the solution of the eikonal equation

$$|\nabla\tau|^2 = \frac{1}{c^2(\vec{\boldsymbol{x}})},$$

and the amplitude α is the solution of the transport equation

$$2\nabla\alpha\cdot\nabla\tau + \alpha\Delta\tau = 0.$$

If the amplitude σ of the fluctuations of the index of refraction is small, then we can expand formally

$$\alpha = \alpha_0 + \sigma\alpha_1 + \sigma^2\alpha_2 + \ldots, \quad \text{and} \quad \tau = \tau_0 + \sigma\tau_1 + \sigma^2\tau_2 + \ldots.$$

Substituting into the eikonal and transport equations, and collecting the terms with the same powers in σ, we find that

$$|\nabla\tau_0| = \frac{1}{c_o}, \qquad \nabla\tau_0\cdot\nabla\tau_1 = \frac{\mu(\vec{\boldsymbol{x}})}{2c_o^2},$$
$$2\nabla\alpha_0\cdot\nabla\tau_0 + \alpha_0\Delta\tau_0 = 0, \qquad 2\nabla\alpha_0\cdot\nabla\tau_1 + 2\nabla\alpha_1\cdot\nabla\tau_0 + \alpha_0\Delta\tau_1 + \alpha_1\Delta\tau_0 = 0.$$

Let us consider the perturbation of a plane wave propagating in the x_{n+1} direction. To leading order we have

$$\alpha_0 = 1, \qquad \tau_0 = \frac{x_{n+1}}{c_o},$$

and the corrections α_1 and τ_1 satisfy

$$\partial_{x_{n+1}}\tau_1 = \frac{\mu(\vec{\boldsymbol{x}})}{2c_o}, \qquad \partial_{x_{n+1}}\alpha_1 = -\frac{c_o}{2}\Delta\tau_1.$$

By splitting the Laplacian as $\Delta = \Delta_\perp + \partial^2_{x_{n+1}}$, we find that the equation for α_1 is equivalent to

$$\partial_{x_{n+1}}\alpha_1 + \frac{1}{4}\partial_{x_{n+1}}\mu = -\frac{c_o}{2}\Delta_\perp\tau_1,$$

which gives for $\vec{\boldsymbol{x}} = (\boldsymbol{0}, L)$,

$$\tau_1 = \frac{1}{2c_o}\int_0^L \mu\left(\frac{s\vec{\boldsymbol{e}}_{n+1}}{\ell}\right) ds, \tag{A.1}$$

$$\alpha_1 = \frac{1}{4}\mu(\boldsymbol{0}) - \frac{1}{4}\mu\left(\frac{L\vec{\boldsymbol{e}}_{n+1}}{\ell}\right) + \tilde{\alpha}_1, \qquad \tilde{\alpha}_1 = -\frac{1}{4\ell^2}\int_0^L (L-s)\Delta_\perp\mu\left(\frac{s\vec{\boldsymbol{e}}_{n+1}}{\ell}\right) ds. \tag{A.2}$$

Here $\vec{\boldsymbol{e}}_{n+1}$ is the unit vector in $\mathbb{R}^{n+1}$ pointing in the x_{n+1} direction.

Our goal is to find under which conditions the random travel time model is valid. This model says that the amplitude perturbation of the wave is negligible, and that the phase (or travel time) perturbation can be described in terms of a Gaussian process with mean zero. In the following lemma the hypothesis $L \gg \ell$ ensures that the statistics of τ_1 is Gaussian by the central limit theorem.

LEMMA A.1. *If the power spectral density $\hat{\mathcal{R}}$ (which is the Fourier transform of $\mathcal{R}$) of the random process μ decays fast enough, and if $x_{n+1} = L \gg \ell$, then*

1. *The travel time correction τ_1 has Gaussian statistics with mean $\mathbb{E}[\tau_1] = 0$ and variance $\mathbb{E}[\tau_1^2]$ of order $(L/c_o)^2(\ell/L)$*

$$\mathbb{E}[\tau_1^2] = \frac{\gamma_0 L^2}{4c_o^2}\frac{\ell}{L}, \qquad \gamma_0 = \frac{1}{(2\pi)^n}\int_{\mathbb{R}^n} \hat{\mathcal{R}}((\boldsymbol{\kappa},0))d\boldsymbol{\kappa}. \tag{A.3}$$

   Recall that $\tau_o = L/c_o$.

2. *The amplitude correction α_1 has Gaussian statistics with mean $\mathbb{E}[\alpha_1] = 0$ and variance $\mathbb{E}[\alpha_1^2]$ of order $(L/\ell)^3$,*

$$\mathbb{E}[\alpha_1^2] = \frac{\gamma_4}{12}\frac{L^3}{\ell^3}, \qquad \gamma_4 = \frac{1}{(2\pi)^n}\int_{\mathbb{R}^n} \hat{\mathcal{R}}((\boldsymbol{\kappa},0))|\boldsymbol{\kappa}|^4 d\boldsymbol{\kappa}. \tag{A.4}$$

Note also that the ratio of the variance of the perturbation of the phase and the variance of the perturbation of the amplitude is $\mathbb{E}[\omega^2\tau_1^2]/\mathbb{E}[\alpha_1^2] \sim \ell^4/(\lambda^2 L^2)$.

Proof. We have

$$\mathbb{E}[\tau_1^2] = \frac{1}{4c_o^2}\int_0^L\int_0^L \mathcal{R}_0\left(\frac{s'-s}{\ell}\right)dsds',$$

where $\mathcal{R}_0$ is the autocorrelation of the stationary process $s \to \mu(s\vec{\boldsymbol{e}}_{n+1})$,

$$\mathcal{R}_0(s'-s) = \mathbb{E}\big[\mu(s\vec{\boldsymbol{e}}_{n+1})\mu(s'\vec{\boldsymbol{e}}_{n+1})\big] = \mathbb{E}\big[\mu(\mathbf{0})\mu((s'-s)\vec{\boldsymbol{e}}_{n+1})\big].$$

Since $\mathcal{R}_o$ is an even function, we obtain

$$\mathbb{E}[\tau_1^2] = \frac{1}{2c_o^2}\int_0^L\int_{\tilde{s}}^L \mathcal{R}_0\left(\frac{\tilde{s}}{\ell}\right)ds\,d\tilde{s} = \frac{1}{2c_o^2}\int_0^L \mathcal{R}_0\left(\frac{s'}{\ell}\right)(L-\tilde{s})d\tilde{s} = \frac{L\ell}{2c_o^2}\int_0^{L/\ell}\left(1-s\frac{\ell}{L}\right)\mathcal{R}_0(s)ds.$$

Since $|(1-s\frac{\ell}{L})\mathcal{R}_0(s)| \le |\mathcal{R}_0(s)|$ for all $s \ge 0$, provided $\mathcal{R}_0 \in L^1(\mathbb{R})$ we obtain by Lebesgue's dominated convergence theorem

$$\frac{2c_o^2}{L\ell}\mathbb{E}[\tau_1^2] = \int_0^{L/\ell}\big(1-s\frac{\ell}{L}\big)\mathcal{R}_0(s)ds \overset{L/\ell\to\infty}{\longrightarrow} \frac{1}{2}\int_{-\infty}^{\infty}\mathcal{R}_0(s)ds.$$

From

$$\mathbb{E}\big[\mu(\vec{\boldsymbol{x}})\mu(\vec{\boldsymbol{x}}')\big] = \mathcal{R}(\vec{\boldsymbol{x}}-\vec{\boldsymbol{x}}') = \frac{1}{(2\pi)^{n+1}}\int_{\mathbb{R}^{n+1}}\hat{\mathcal{R}}(\vec{\boldsymbol{\kappa}})e^{i\vec{\boldsymbol{\kappa}}\cdot(\vec{\boldsymbol{x}}-\vec{\boldsymbol{x}}')}d\vec{\boldsymbol{\kappa}}, \tag{A.5}$$

we obtain

$$\mathcal{R}_0(s) = \mathcal{R}(s\vec{\boldsymbol{e}}_{n+1}) = \frac{1}{(2\pi)^{n+1}}\int_{\mathbb{R}^{n+1}}\hat{\mathcal{R}}(\vec{\boldsymbol{\kappa}})e^{i\kappa_{n+1}s}d\vec{\boldsymbol{\kappa}},$$

which gives result (A.3) after integrating in s.

The Gaussian property is straightforward if μ is Gaussian. In the case that μ is not Gaussian, it follows from a form of the central limit theorem under strong mixing applied to the process $s \to \mu(s\vec{\boldsymbol{e}}_{n+1}/\ell)$ when the process is strongly mixing and admits high-order moments. We have

$$\mathbb{E}[\tilde{\alpha}_1^2] = \frac{1}{4\ell^4}\int_0^L \int_0^L (L-s)(L-s')\mathcal{R}_4\big(\frac{s'-s}{\ell}\big)dsds',$$

where $\tilde{\alpha}_1$ is defined in (A.2) and $\mathcal{R}_4$ is the correlation function of $s \to \Delta_\perp\mu(s\vec{\boldsymbol{e}}_{n+1})$,

$$\mathcal{R}_4(s-s') = \mathbb{E}\big[\Delta_\perp\mu(s\vec{\boldsymbol{e}}_{n+1})\Delta_\perp\mu(s'\vec{\boldsymbol{e}}_{n+1})\big] = \mathbb{E}\big[\Delta_\perp\mu(\mathbf{0})\Delta_\perp\mu((s'-s)\vec{\boldsymbol{e}}_{n+1})\big],$$

Using standard algebraic manipulations and the fact that $\mathcal{R}_4$ is an even function, we obtain

$$\mathbb{E}[\tilde{\alpha}_1^2] = \frac{1}{4\ell^4}\int_0^L \int_0^L ss'\mathcal{R}_4\left(\frac{s'-s}{\ell}\right)ds'ds = \frac{L^3}{6\ell^3}\int_0^{L/\ell}\left(1 - s\frac{3\ell}{2L} + s^3\frac{\ell^3}{2L^3}\right)\mathcal{R}_4(s)ds.$$

Since $|(1 - s\frac{3\ell}{2L} + s^3\frac{\ell^3}{2L^3})\mathcal{R}_4(s)| \le |\mathcal{R}_4(s)|$ for all $s \ge 0$, provided $\mathcal{R}_4 \in L^1(\mathbb{R})$ we obtain by Lebesgue's dominated convergence theorem that

$$\frac{\ell^3}{L^3}\mathbb{E}[\tilde{a}_1^2] = \frac{1}{6}\int_0^{L/\ell}\big(1 - s\frac{3\ell}{2L} + s^3\frac{\ell^3}{2L^3}\big)\mathcal{R}_4(s)ds \overset{L/\ell\to\infty}{\longrightarrow} \frac{1}{12}\int_{-\infty}^{\infty}\mathcal{R}_4(s)ds.$$

We also obtain from (A.5), with $\vec{\boldsymbol{\kappa}} = (\boldsymbol{\kappa}, \kappa_{n+1})$, that

$$\mathcal{R}_4(s) = \Delta_\perp^2\mathcal{R}(s\vec{\boldsymbol{e}}_{n+1}) = \frac{1}{(2\pi)^{n+1}}\int_{\mathbb{R}^{n+1}}|\boldsymbol{\kappa}|^4\hat{\mathcal{R}}(\vec{\boldsymbol{\kappa}})e^{i\kappa_{n+1}s}d\vec{\boldsymbol{\kappa}}.$$

This gives the result (A.4), after integrating in s and noting that

$$1 \sim \mathbb{E}[(\alpha_1 - \tilde{\alpha}_1)^2] \ll \mathbb{E}[\tilde{\alpha}_1^2] \sim (L/\ell)^3.$$

□

The second order term τ_2 in the expansion of the travel time satisfies the equation

$$2\nabla\tau_0\cdot\nabla\tau_2 + |\nabla\tau_1|^2 = 0,$$

which gives

$$\tau_2 = -\frac{1}{8c_o}\int_0^L \mu^2\big(\frac{s\vec{\boldsymbol{e}}_{n+1}}{\ell}\big)ds - \frac{1}{8c_o\ell^2}\int_0^L\Big|\int_0^s\nabla_\perp\mu\big(\frac{s'\vec{\boldsymbol{e}}_{n+1}}{\ell}\big)ds'\Big|^2ds.$$

Its mean and variance are given by the next lemma. Its proof involves calculations that are similar to those given above, and are not included here.

LEMMA A.2. *Under the same assumptions as in Lemma A.1, we have*

$$\mathbb{E}[\tau_2] = -\frac{\gamma_0 L^2}{16c_o\ell}, \qquad \mathrm{Var}(\tau_2) = \frac{8}{3}\Big(\frac{\gamma_0 L^2}{16c_o\ell}\Big)^2. \tag{A.6}$$

For the random travel time model to be valid, the wavelength λ, the correlation length ℓ, the propagation distance L, and the standard deviation σ of the fluctuations of the index of refraction should fulfill the following conditions:

- The geometric optics approximation should be valid, so we should have $\lambda \ll \ell$.
- The statistics of the phase should be Gaussian, so we should have $\ell \ll L$.
- The amplitude of the fluctuations of the index of refraction should be small, $\sigma \ll 1$.
- The amplitude perturbation α_1 of the wave should be small. By (A.4) we should have $\sigma^2 \frac{L^3}{\ell^3} \ll 1$.
- The perturbation of the phase $\omega\tau_1$ of the wave should be of order one (or larger). By (A.3) we should have $\sigma^2 \frac{L\ell}{\lambda^2} \sim 1$ (or > 1).
- The phase should be accurately described by the expansion $\omega(\tau_0 + \sigma\tau_1)$. This holds if the next term in the expansion of the phase is negligible. By (A.6) the phase term $\omega\tau_2$ is negligible if $\sigma^2 \frac{L^2}{\lambda\ell} \ll 1$.

All these conditions are fulfilled if

$$\frac{\ell}{L} \ll 1, \qquad \sigma^2 \ll \frac{\ell^3}{L^3}, \qquad \sigma^2 \frac{L^3}{\ell^3} \ll \frac{\lambda^2}{\sigma^2 \ell L} \lesssim 1. \tag{A.7}$$

Note that, since $\sigma^2 \frac{L^3}{\ell^3} \ll 1$, the last condition can be fulfilled by a large range of values of λ. Note also that we could consider a more general version of the random travel time model: We could relax the condition that the perturbation of the phase of the wave should be at least of order one, but this would mean that the random fluctuations of the medium induce no amplitude neither phase perturbation of the wave. We could also relax the condition that the travel time correction τ_2 should be negligible, but this would mean that the travel time statistics is more complicated than the one considered in the paper.

Appendix B. Variance of KM with passive arrays. To compute the variance of (4.11), we use the second moment (3.19). We have

$$\mathbb{E}\left\{|\mathcal{I}^{\mathrm{KM}}(\vec{\boldsymbol{y}})|^2\right\} \approx |\alpha(L,\omega_o)|^2 \int_{\mathcal{A}} d\boldsymbol{x} \int_{\mathcal{A}} d\boldsymbol{x}' \int_{-\infty}^{\infty} \frac{d\omega}{2\pi}\, \widehat{f}(\omega) \int_{-\infty}^{\infty} \frac{d\omega'}{2\pi}\, \overline{\widehat{f}(\omega')}\, e^{-\frac{(\omega-\omega')^2\tau_c^2}{2} - \frac{|\boldsymbol{x}-\boldsymbol{x}'|^2}{2X_c^2}}, \tag{B.1}$$

whereas

$$|\mathcal{I}_o^{\mathrm{KM}}(\vec{\boldsymbol{y}})| = |\alpha(L,\omega_o)|^2\, a^{2n}. \tag{B.2}$$

Not let us change variables $\boldsymbol{x}' \rightsquigarrow \widetilde{\boldsymbol{x}} = \boldsymbol{x}' - \boldsymbol{x}$, and use that $X_c \ll \ell \lesssim a$, to approximate the spatial integrals as

$$\int_{\mathcal{A}} d\boldsymbol{x} \int_{\mathcal{A}} d\boldsymbol{x}' e^{-\frac{|\boldsymbol{x}-\boldsymbol{x}'|^2}{2X_c^2}} \approx \int_{\mathcal{A}} d\boldsymbol{x} \int_{\mathbb{R}^n} e^{-\frac{|\widetilde{\boldsymbol{x}}|^2}{2X_c^2}} = \left(\sqrt{2\pi} a X_c\right)^n. \tag{B.3}$$

For the integrals over the frequencies, we recall the Gaussian pulse (2.3), and change variables $\omega' \rightsquigarrow \omega + \widetilde{\omega}$, to obtain

$$\begin{aligned}\int_{-\infty}^{\infty} \frac{d\omega}{2\pi}\, \widehat{f}(\omega) \int_{-\infty}^{\infty} \frac{d\omega'}{2\pi}\, \overline{\widehat{f}(\omega')}\, e^{-\frac{(\omega-\omega')^2\tau_c^2}{2}} &= \frac{1}{2\pi B^2} \int_{-\infty}^{\infty} d\omega \int_{-\infty}^{\infty} d\widetilde{\omega}\, e^{-\frac{(\omega-\omega_o)^2}{2B^2} - \frac{(\omega-\omega_o+\widetilde{\omega})^2}{2B^2} - \frac{\widetilde{\omega}^2\tau_c^2}{2}} \\ &= \frac{1}{\sqrt{1+2B^2\tau_c^2}}.\end{aligned} \tag{B.4}$$

Equation (4.19) follows from (B.1)-(B.4). □.

Appendix C. Proof of Proposition 4.2. After the change of variables $\boldsymbol{x} = \frac{\boldsymbol{x}_r + \boldsymbol{x}_r'}{2}$, $\widetilde{\boldsymbol{x}} = \boldsymbol{x}_r - \boldsymbol{x}_r'$, and $\omega \rightsquigarrow \frac{\omega+\omega'}{2}$, $\widetilde{\omega} = \omega - \omega'$, we obtain from (4.21) that

$$\begin{aligned}\mathcal{I}^{\mathrm{CINT}}(\vec{\boldsymbol{y}}^S) = \int_{\mathcal{A}} d\boldsymbol{x} \int_{\mathbb{R}^n} d\widetilde{\boldsymbol{x}} \int_{-\infty}^{\infty} \frac{d\omega}{2\pi} \int_{-\infty}^{\infty} \frac{d\widetilde{\omega}}{2\pi} \widehat{\Phi}\left(\frac{\widetilde{\omega}}{\Omega_d}\right) \Psi\left(\frac{\widetilde{\boldsymbol{x}}}{X_d}\right) \int_{\mathbb{R}^n} \frac{d\boldsymbol{\kappa}}{(2\pi)^n} \int_{-\infty}^{\infty} \frac{dT}{2\pi}\, W(\omega, \boldsymbol{x}; \boldsymbol{\kappa}, T) \\ \times \exp\left\{-i\widetilde{\boldsymbol{x}} \cdot \left[\boldsymbol{\kappa} - \frac{\omega_o}{c_o} \frac{(\boldsymbol{\xi} - \boldsymbol{x})}{L}\right] + i\widetilde{\omega}\left[T - \tau_o(\vec{\boldsymbol{x}}, \vec{\boldsymbol{y}}^S)\right]\right\}.\end{aligned} \tag{C.1}$$

We extended the integral in $\widetilde{\boldsymbol{x}}$ to $\mathbb{R}^n$, because $\widetilde{\boldsymbol{x}}$ is restricted by the essential support X_d of the Gaussian window Ψ. This is assuming $X_d < a$. We also dropped the terms

$$\frac{(\omega-\omega_o)}{c_o}\frac{\boldsymbol{x}\cdot\widetilde{\boldsymbol{x}}}{L} \sim \frac{B}{\omega_o}\frac{X_d}{\lambda_o L/a}, \qquad \frac{\widetilde{\omega}|\widetilde{\boldsymbol{x}}|^2}{c_o L} \sim \frac{\Omega_d}{\omega_o}\frac{X_d^2}{\lambda_o L},$$

based on the assumptions (4.23), and used (4.5) to get

$$\frac{\widetilde{\omega}}{c_o}\frac{\boldsymbol{x}\cdot\boldsymbol{\xi}}{L} \sim \frac{\Omega_d}{\omega_o}\frac{|\boldsymbol{\xi}|}{\lambda_o L/a} \ll \frac{\Omega_d}{B} \lesssim O(1).$$

Now we substitute in (C.1) the Gaussian windows (2.14), integrate over $\widetilde{\boldsymbol{x}}$ and $\widetilde{\omega}$ and obtain

$$\mathcal{I}^{\text{CINT}}(\vec{\boldsymbol{y}}^S) = \frac{\Omega_d X_d^n}{(2\pi)^{\frac{n+5}{2}}}\int_{\mathcal{A}} d\boldsymbol{x}\int_{-\infty}^{\infty} d\omega \int_{\mathbb{R}^n} d\boldsymbol{\kappa}\int_{-\infty}^{\infty} dT\, W(\omega,\boldsymbol{x};\boldsymbol{\kappa},T)$$
$$\times\exp\left\{-\frac{\Omega_d^2\left[T-\tau_o(\vec{\boldsymbol{x}},\vec{\boldsymbol{y}})\right]^2}{2} - \frac{X_d^2\left|\boldsymbol{\kappa}-\frac{\omega_o}{c_o}\frac{(\boldsymbol{\xi}-\boldsymbol{x})}{L}\right|^2}{2}\right\}, \tag{C.2}$$

as stated in Proposition 4.2. □.

Appendix D. Proof of Propositions 4.3 and 4.4. Recall definitions (4.7)-(4.22), the random travel time model (4.8), and the approximation (4.4) of the travel time, to write

$$\mathbb{E}\left\{W(\omega,\boldsymbol{x};\boldsymbol{\kappa},T)\right\} \approx |\alpha(L,\omega_o)|^2\int_{\mathbb{R}^n} d\widetilde{\boldsymbol{x}}\int_{-\infty}^{\infty} d\widetilde{\omega}\,\widehat{f}\left(\omega+\frac{\widetilde{\omega}}{2}\right)\overline{\widehat{f}\left(\omega-\frac{\widetilde{\omega}}{2}\right)}\,\mathbb{E}\left\{e^{i\left(\omega+\frac{\widetilde{\omega}}{2}\right)\nu\left(\boldsymbol{x}+\frac{\widetilde{\boldsymbol{x}}}{2}\right)-i\left(\omega-\frac{\widetilde{\omega}}{2}\right)\nu\left(\boldsymbol{x}-\frac{\widetilde{\boldsymbol{x}}}{2}\right)}\right\}$$
$$\times\exp\left\{i\widetilde{\omega}\tau_o(\vec{\boldsymbol{x}},\vec{\boldsymbol{y}}) + i\frac{\omega_o}{c_o}\frac{\widetilde{\boldsymbol{x}}\cdot\boldsymbol{x}}{L} + i\boldsymbol{\kappa}\cdot\widetilde{\boldsymbol{x}} - i\widetilde{\omega}T\right\}. \tag{D.1}$$

Here we neglected two terms in the phase,

$$\frac{\widetilde{\omega}}{c_o}\frac{|\widetilde{\boldsymbol{x}}|^2}{8L} \sim \frac{\Omega_c}{\omega_o}\frac{X_c^2}{\lambda_o L}, \quad \text{and} \quad \frac{(\omega-\omega_o)}{c_o}\frac{\widetilde{\boldsymbol{x}}\cdot\boldsymbol{x}}{L} \sim \frac{B}{\omega_o}\frac{X_c}{\lambda_o L/a},$$

by the assumptions (4.25), and the fact that the mean in (D.1) is supported at frequencies $|\widetilde{\omega}| \lesssim \Omega_c = 1/\tau_c$, and at offsets $|\widetilde{\boldsymbol{x}}| \lesssim X_c$, as seen from equation (3.19). Substituting in (D.1) the Gaussian expression (2.3) of the pulse, and the moment formula (3.19), we obtain after integrating in $\widetilde{\boldsymbol{x}}$ and $\widetilde{\omega}$ the expression of the mean of the Wigner transform stated in Proposition 4.2.

The mean of $\mathcal{I}^{\text{CINT}}(\vec{\boldsymbol{y}}^S)$ follows from (4.24) and (4.26),

$$\mathbb{E}\left\{\mathcal{I}^{\text{CINT}}(\vec{\boldsymbol{y}}^S)\right\} \approx \frac{|\alpha(L,\omega_o)|^2\Omega_d(X_dX_c)^n}{2\pi B^2}\sqrt{\frac{2B^2}{1+2B^2\tau_c^2}}\int_{\mathcal{A}} d\boldsymbol{x}\int_{-\infty}^{\infty} d\omega\, e^{-\frac{(\omega-\omega_o)^2}{B^2}}\int_{\mathbb{R}^n} d\boldsymbol{\kappa}\int_{-\infty}^{\infty} dT$$
$$\times\exp\left\{-\frac{\Omega_d^2\left(T-\Delta\tau_o\right)^2}{2} - \frac{T^2}{2}\left(\frac{2B^2}{1+2B^2\tau_c^2}\right) - \frac{X_c^2|\boldsymbol{\kappa}|^2}{2} - \frac{X_d^2\left|\boldsymbol{\kappa}-\frac{\omega_o}{c_o}\frac{\boldsymbol{\xi}}{L}\right|^2}{2}\right\}. \tag{D.2}$$

Here we used the Gaussian expression of the pulse, changed variables $\boldsymbol{\kappa} \rightsquigarrow \boldsymbol{\kappa} + \frac{\omega_o}{c_o}\frac{\boldsymbol{x}}{L}$, $T \rightsquigarrow T - \tau_o(\vec{\boldsymbol{x}},\vec{\boldsymbol{y}})$, and introduced the difference in travel times

$$\Delta\tau_o = \tau_o(\vec{\boldsymbol{x}},\vec{\boldsymbol{y}}^S) - \tau_o(\vec{\boldsymbol{x}},\vec{\boldsymbol{y}}). \tag{D.3}$$

We write next $\Delta\tau_o$ using (4.6),

$$\Omega_d \Delta\tau_o \approx \frac{\Omega_d \eta}{c_o} - \frac{\Omega_d}{c_o}\frac{\boldsymbol{x}\cdot\boldsymbol{\xi}}{L} \approx \frac{\Omega_d \eta}{c_o}, \tag{D.4}$$

where the last approximation follows from (4.5),

$$\frac{\Omega_d}{c_o}\frac{\boldsymbol{x}\cdot\boldsymbol{\xi}}{L} \sim \frac{\Omega_d}{\omega_o}\frac{|\boldsymbol{\xi}|}{\lambda_o L/a} \ll \frac{\Omega_d}{B} \lesssim 1.$$

The result follows by carrying out the integrals in (D.2). □.

Appendix E. Variance of CINT with passive arrays. The autocorrelation of $\mathcal{I}^{\text{CINT}}(\vec{\boldsymbol{y}})$ involves the fourth order moment of the process $\exp(i\omega\nu(\boldsymbol{x}_r))$. Let us consider four points $(\boldsymbol{x}_j)_{j=1,\dots,4}$ in $\mathcal{A}$ and four frequencies $(\omega_j)_{j=1,\dots,4}$ in the bandwidth. Using the Gaussian property of the process $\nu(\boldsymbol{x})$ and the fact that $\mathcal{C}(0)=1$, we have

$$\mathbb{E}\big[e^{i\omega_1\nu(\boldsymbol{x}_1)-i\omega_2\nu(\boldsymbol{x}_2)}\overline{e^{i\omega_3\nu(\boldsymbol{x}_3)-i\omega_4\nu(\boldsymbol{x}_4)}}\big] = \exp\Big\{-\frac{\tau_c^2}{2}\Big[\sum_{j=1}^4\omega_j^4 + 2\omega_1\omega_4\mathcal{C}\left(\frac{|\boldsymbol{x}_1-\boldsymbol{x}_4|}{\ell}\right) + 2\omega_2\omega_3\mathcal{C}\left(\frac{|\boldsymbol{x}_2-\boldsymbol{x}_3|}{\ell}\right)$$
$$-2\omega_1\omega_2\mathcal{C}\left(\frac{|\boldsymbol{x}_1-\boldsymbol{x}_2|}{\ell}\right) - 2\omega_1\omega_3\mathcal{C}\left(\frac{|\boldsymbol{x}_1-\boldsymbol{x}_3|}{\ell}\right) - 2\omega_2\omega_4\mathcal{C}\left(\frac{|\boldsymbol{x}_2-\boldsymbol{x}_4|}{\ell}\right) - 2\omega_3\omega_4\mathcal{C}\left(\frac{|\boldsymbol{x}_3-\boldsymbol{x}_4|}{\ell}\right)\Big]\Big\}.$$

In fact we are only interested in the forth-order moment for which the points and frequencies are of the form

$$\omega_1 = \omega + \frac{\widetilde{\omega}}{2}, \quad \omega_2 = \omega - \frac{\widetilde{\omega}}{2}, \qquad \omega_3 = \omega' + \frac{\widetilde{\omega}'}{2}, \quad \omega_4 = \omega' - \frac{\widetilde{\omega}'}{2},$$
$$\boldsymbol{x}_1 = \boldsymbol{x} + \frac{\widetilde{\boldsymbol{x}}}{2}, \quad \boldsymbol{x}_2 = \boldsymbol{x} - \frac{\widetilde{\boldsymbol{x}}}{2}, \qquad \boldsymbol{x}_3 = \boldsymbol{x}' + \frac{\widetilde{\boldsymbol{x}}'}{2}, \quad \boldsymbol{x}_4 = \boldsymbol{x}' - \frac{\widetilde{\boldsymbol{x}}'}{2},$$

with $\omega,\omega' = O(\omega_o)$; $\widetilde{\omega},\widetilde{\omega}' = O(\Omega_d)$; $\boldsymbol{x},\boldsymbol{x}' = O(a)$; $\widetilde{\boldsymbol{x}},\widetilde{\boldsymbol{x}}' = O(X_d)$. If $X_d \ll \ell$, then the expression of the forth-order moment can be simplified into

$$\mathbb{E}\big[e^{i\omega_1\nu(\boldsymbol{x}_1)-i\omega_2\nu(\boldsymbol{x}_2)}\overline{e^{i\omega_3\nu(\boldsymbol{x}_3)-i\omega_4\nu(\boldsymbol{x}_4)}}\big] = \exp\Big\{-\frac{\tau_c^2}{2}\Big[\widetilde{\omega}^2+\widetilde{\omega}'^2 - 2\widetilde{\omega}\widetilde{\omega}'\mathcal{C}\left(\frac{|\boldsymbol{x}-\boldsymbol{x}'|}{\ell}\right)\Big]\Big\}.$$

Note that a sufficient condition for $X_d \ll \ell$ is that $X_d \sim X_c$ since $X_c \ll \ell$ by Eq. (3.20). This condition can be readilly fulfilled because we have already shown that the expectation of the CINT functional and the resolution analysis are not affected as long as $X_d \geq X_c$, so we can restrict the analysis to the second-order moment to the case $X_d \sim X_c \ll \ell$.

Substituting the model (4.7) of the array data in (4.21) and using the Gaussian pulse and Gaussian windows, we have

$$\mathbb{E}\big[\mathcal{I}^{\text{CINT}}(\vec{\boldsymbol{y}})\overline{\mathcal{I}^{\text{CINT}}(\vec{\boldsymbol{y}})}\big] = \frac{|\alpha(L,\omega_o)|^4}{4\pi B^2}\int_{\mathcal{A}}d\boldsymbol{x}\int_{-\infty}^{\infty}d\widetilde{\omega}\int_{\mathbb{R}^n}d\widetilde{\boldsymbol{x}}\int_{\mathcal{A}}d\boldsymbol{x}'\int_{-\infty}^{\infty}d\widetilde{\omega}'\int_{\mathbb{R}^n}d\widetilde{\boldsymbol{x}}'\ \exp\Big[\tau_c^2\widetilde{\omega}\widetilde{\omega}'\mathcal{C}\left(\frac{|\boldsymbol{x}-\boldsymbol{x}'|}{\ell}\right)$$
$$-\frac{(\widetilde{\omega}^2+\widetilde{\omega}'^2)}{2}\left(\tau_c^2+\frac{1}{\Omega_d^2}+\frac{1}{2B^2}\right) - \frac{(|\widetilde{\boldsymbol{x}}|^2+|\widetilde{\boldsymbol{x}}'|^2)}{2}\left(\frac{1}{X_d^2}+\frac{1}{X_c^2}\right)\Big],$$

whereas

$$\mathbb{E}\big[\mathcal{I}^{\text{CINT}}(\vec{\boldsymbol{y}})\big] = \frac{|\alpha(L,\omega_o)|^2}{2\sqrt{\pi}B}\int_{\mathcal{A}}d\boldsymbol{x}\int_{-\infty}^{\infty}d\widetilde{\omega}\int_{\mathbb{R}^n}d\widetilde{\boldsymbol{x}}\exp\Big[-\frac{\widetilde{\omega}^2}{2}\left(\tau_c^2+\frac{1}{\Omega_d^2}+\frac{1}{2B^2}\right) - \frac{|\widetilde{\boldsymbol{x}}|^2}{2}\left(\frac{1}{X_d^2}+\frac{1}{X_c^2}\right)\Big].$$

Moreover, using that

$$\exp\Big[\tau_c^2\widetilde{\omega}\widetilde{\omega}'\mathcal{C}\left(\frac{|\boldsymbol{x}-\boldsymbol{x}'|}{\ell}\right)\Big]-1\simeq\Big[\tau_c^2\widetilde{\omega}\widetilde{\omega}'\mathcal{C}\left(\frac{|\boldsymbol{x}-\boldsymbol{x}'|}{\ell}\right)\Big]+\frac{1}{2}\Big[\tau_c^2\widetilde{\omega}\widetilde{\omega}'\mathcal{C}\left(\frac{|\boldsymbol{x}-\boldsymbol{x}'|}{\ell}\right)\Big]^2,$$

which holds if $\Omega_d \ll \tau_c^{-1}$, we obtain the variance

$$\begin{aligned}\mathrm{Var}\big(\mathcal{I}^{\mathrm{CINT}}(\vec{\boldsymbol{y}})\big)&=\frac{|\alpha(L,\omega_o)|^4}{8\pi B^2}\left\{\int_{\mathbb{R}^n}d\widetilde{\boldsymbol{x}}\,\exp\left[-\frac{|\widetilde{\boldsymbol{x}}|^2}{2}\left(\frac{1}{X_d^2}+\frac{1}{X_c^2}\right)\right]\right\}^2\\&\times\left\{\tau_c^2\int d\widetilde{\omega}\,\widetilde{\omega}^2\exp\left[-\frac{h^2}{2}\left(\tau_c^2+\frac{1}{\Omega_d^2}+\frac{1}{2B^2}\right)\right]\right\}^2\left\{\int_{\mathcal{A}}d\boldsymbol{x}\int_{\mathcal{A}}d\boldsymbol{x}'\,\mathcal{C}\left(\frac{|\boldsymbol{x}-\boldsymbol{x}'|}{\ell}\right)^2\right\}\end{aligned}$$

and therefore

$$\mathrm{Var}\left[\mathcal{I}^{\mathrm{CINT}}(\vec{\boldsymbol{y}})\right]=\frac{1}{2}\left(\frac{\tau_c^2}{\tau_c^2+\frac{1}{\Omega_d^2}+\frac{1}{2B^2}}\right)^2\left[\frac{1}{a^{2n}}\int_{\mathcal{A}}d\boldsymbol{x}\int_{\mathcal{A}}d\boldsymbol{x}'\,\mathcal{C}\left(\frac{|\boldsymbol{x}-\boldsymbol{x}'|}{\ell}\right)^2\right]\left|\mathbb{E}\big[\mathcal{I}^{\mathrm{CINT}}(\vec{\boldsymbol{y}})\big]\right|^2.$$

This is the variance stated in Proposition 4.5. □.

Appendix F. Proof of proposition 5.1. Let us begin with definition (5.8) of $\mathcal{I}^{\mathrm{CINT}}(\vec{\boldsymbol{y}}^S)$, and note that

$$\hat{p}(\omega,\boldsymbol{x}_r,\boldsymbol{x}_s)=\widehat{\mathcal{P}}(\omega,\boldsymbol{x}_r)\widehat{\mathcal{P}}(\omega,\boldsymbol{x}_s). \tag{F.1}$$

Changing the receiver variables $\frac{\boldsymbol{x}_r+\boldsymbol{x}_r'}{2}\rightsquigarrow\boldsymbol{x}_r$, $\boldsymbol{x}_r-\boldsymbol{x}_r'=\widetilde{\boldsymbol{x}}_r$, and similar for the sources, and introducing the central and difference frequencies $\frac{\omega+\omega'}{2}\rightsquigarrow\omega$, $\omega-\omega'=\widetilde{\omega}$, we have

$$\begin{aligned}\mathcal{I}^{\mathrm{CINT}}(\vec{\boldsymbol{y}}^S)=\int_{\mathcal{A}}d\boldsymbol{x}_r\int_{\mathcal{A}}d\boldsymbol{x}_s\int_{-\infty}^{\infty}\frac{d\omega}{2\pi}\int d\widetilde{\boldsymbol{x}}_r\Psi\left(\frac{\widetilde{\boldsymbol{x}}_r}{X_d}\right)\int d\widetilde{\boldsymbol{x}}_s\Psi\left(\frac{\widetilde{\boldsymbol{x}}_s}{X_d}\right)\int_{-\infty}^{\infty}\frac{d\widetilde{\omega}}{2\pi}\widehat{\Phi}\left(\frac{\widetilde{\omega}}{\Omega_d}\right)\\\times\widehat{\mathcal{P}}\left(\omega+\frac{\widetilde{\omega}}{2},\boldsymbol{x}_r+\frac{\widetilde{\boldsymbol{x}}_r}{2}\right)\overline{\widehat{\mathcal{P}}\left(\omega-\frac{\widetilde{\omega}}{2},\boldsymbol{x}_r-\frac{\widetilde{\boldsymbol{x}}_r}{2}\right)}\widehat{\mathcal{P}}\left(\omega+\frac{\widetilde{\omega}}{2},\boldsymbol{x}_s+\frac{\widetilde{\boldsymbol{x}}_s}{2}\right)\overline{\widehat{\mathcal{P}}\left(\omega-\frac{\widetilde{\omega}}{2},\boldsymbol{x}_s-\frac{\widetilde{\boldsymbol{x}}_s}{2}\right)}\\\times\exp\left\{-i\omega\left[\Delta\tau_o(\boldsymbol{x}_r,\widetilde{\boldsymbol{x}}_r,\vec{\boldsymbol{y}}^S)+\Delta\tau_o(\boldsymbol{x}_s,\widetilde{\boldsymbol{x}}_s,\vec{\boldsymbol{y}}^S)\right]-i\widetilde{\omega}\left[\langle\tau_o\rangle(\boldsymbol{x}_r,\widetilde{\boldsymbol{x}}_r,\vec{\boldsymbol{y}}^S)+\langle\tau_o\rangle(\boldsymbol{x}_s,\widetilde{\boldsymbol{x}}_s,\vec{\boldsymbol{y}}^S)\right]\right\}.\end{aligned} \tag{F.2}$$

Here we let

$$\begin{aligned}\Delta\tau_o(\boldsymbol{x}_r,\widetilde{\boldsymbol{x}}_r,\vec{\boldsymbol{y}}^S)&=\tau_o\left((\boldsymbol{x}_r+\frac{\widetilde{\boldsymbol{x}}_r}{2},0),\vec{\boldsymbol{y}}^S\right)-\tau_o\left((\boldsymbol{x}_r-\frac{\widetilde{\boldsymbol{x}}_r}{2},0),\vec{\boldsymbol{y}}^S\right)\approx\frac{\widetilde{\boldsymbol{x}}_r\cdot(\boldsymbol{x}_r-\boldsymbol{\xi})}{c_oL},\\\langle\tau_o\rangle(\boldsymbol{x}_r,\widetilde{\boldsymbol{x}}_r,\vec{\boldsymbol{y}}^S)&=\frac{1}{2}\left[\tau_o\left((\boldsymbol{x}_r+\frac{\widetilde{\boldsymbol{x}}_r}{2},0),\vec{\boldsymbol{y}}^S\right)+\tau_o\left((\boldsymbol{x}_r-\frac{\widetilde{\boldsymbol{x}}_r}{2},0),\vec{\boldsymbol{y}}^S\right)\right]\approx\tau_o(\vec{\boldsymbol{x}}_r,\vec{\boldsymbol{y}}^S)+\frac{|\widetilde{\boldsymbol{x}}|^2}{8c_oL},\end{aligned}$$

and used the approximation (4.6) of the travel time. By the assumption (4.23), we have

$$\frac{\omega}{c_o}\frac{\widetilde{\boldsymbol{x}}_r\cdot(\boldsymbol{x}_r-\boldsymbol{\xi})}{L}=\frac{\omega_o}{c_o}\frac{\widetilde{\boldsymbol{x}}_r\cdot(\boldsymbol{x}_r-\boldsymbol{\xi})}{L}+O\left(\frac{B}{\omega_o}\frac{X_d}{\lambda_oL/a}\right)\approx\frac{\omega_o}{c_o}\frac{\widetilde{\boldsymbol{x}}_r\cdot(\boldsymbol{x}_r-\boldsymbol{\xi})}{L},$$

and

$$\widetilde{\omega}\left[\tau_o(\vec{\boldsymbol{x}}_r,\vec{\boldsymbol{y}}^S)+\frac{|\widetilde{\boldsymbol{x}}|^2}{8c_oL}\right]=\widetilde{\omega}\tau_o(\vec{\boldsymbol{x}}_r,\vec{\boldsymbol{y}}^S)+O\left(\frac{\Omega_d}{\omega_o}\frac{X_d^2}{\lambda_oL}\right)\approx\widetilde{\omega}\tau_o(\vec{\boldsymbol{x}}_r,\vec{\boldsymbol{y}}^S),$$

so (F.2) becomes

$$\begin{aligned}\mathcal{I}^{\mathrm{CINT}}(\vec{\boldsymbol{y}}^S)\approx\int_{\mathcal{A}}d\boldsymbol{x}_r\int_{\mathcal{A}}d\boldsymbol{x}_s\int_{-\infty}^{\infty}\frac{d\omega}{2\pi}\int d\widetilde{\boldsymbol{x}}_r\Psi\left(\frac{\widetilde{\boldsymbol{x}}_r}{X_d}\right)\int d\widetilde{\boldsymbol{x}}_s\Psi\left(\frac{\widetilde{\boldsymbol{x}}_s}{X_d}\right)\int_{-\infty}^{\infty}\frac{d\widetilde{\omega}}{2\pi}\widehat{\Phi}\left(\frac{\widetilde{\omega}}{\Omega_d}\right)\\\times\widehat{\mathcal{P}}\left(\omega+\frac{\widetilde{\omega}}{2},\boldsymbol{x}_r+\frac{\widetilde{\boldsymbol{x}}_r}{2}\right)\overline{\widehat{\mathcal{P}}\left(\omega-\frac{\widetilde{\omega}}{2},\boldsymbol{x}_r-\frac{\widetilde{\boldsymbol{x}}_r}{2}\right)}e^{-i\frac{\omega_o}{c_o}\frac{\widetilde{\boldsymbol{x}}_r\cdot(\boldsymbol{x}_r-\boldsymbol{\xi})}{L}-i\widetilde{\omega}\tau_o(\vec{\boldsymbol{x}}_r,\vec{\boldsymbol{y}}^S)}\\\times\widehat{\mathcal{P}}\left(\omega+\frac{\widetilde{\omega}}{2},\boldsymbol{x}_s+\frac{\widetilde{\boldsymbol{x}}_s}{2}\right)\overline{\widehat{\mathcal{P}}\left(\omega-\frac{\widetilde{\omega}}{2},\boldsymbol{x}_s-\frac{\widetilde{\boldsymbol{x}}_s}{2}\right)}e^{-i\frac{\omega_o}{c_o}\frac{\widetilde{\boldsymbol{x}}_s\cdot(\boldsymbol{x}_s-\boldsymbol{\xi})}{L}-i\widetilde{\omega}\tau_o(\vec{\boldsymbol{x}}_s,\vec{\boldsymbol{y}}^S)}.\end{aligned} \tag{F.3}$$

Now let us write $\widehat{\mathcal{P}}\overline{\widehat{\mathcal{P}}}$ in terms of the Wigner transform, and use the Gaussian windows to obtain

$$\mathcal{I}^{\rm CINT}(\vec{\boldsymbol{y}}^S) \approx \frac{1}{(2\pi)^{2n+4}} \int_{\mathcal{A}} d\boldsymbol{x}_r \int_{\mathcal{A}} d\boldsymbol{x}_s \int_{-\infty}^{\infty} d\omega \int d\boldsymbol{\kappa}_r \int dT_r\, \mathcal{W}(\omega, \boldsymbol{x}_r; \boldsymbol{\kappa}_r, T_r) \int d\boldsymbol{\kappa}_s \int dT_s\, \mathcal{W}(\omega, \boldsymbol{x}_s; \boldsymbol{\kappa}_s, T_s)$$
$$\times \int d\widetilde{\boldsymbol{x}}_r\, e^{-\frac{|\widetilde{\boldsymbol{x}}_r|^2}{2X_d^2} - i\widetilde{\boldsymbol{x}}_r \cdot \left(\boldsymbol{\kappa}_r - \frac{\omega_o}{c_o}\frac{(\boldsymbol{\xi}-\boldsymbol{x}_r)}{L}\right)} \int d\widetilde{\boldsymbol{x}}_s\, e^{-\frac{|\widetilde{\boldsymbol{x}}_s|^2}{2X_d^2} - i\widetilde{\boldsymbol{x}}_r \cdot \left(\boldsymbol{\kappa}_s - \frac{\omega_o}{c_o}\frac{(\boldsymbol{\xi}-\boldsymbol{x}_s)}{L}\right)}$$
$$\times \int d\widetilde{\omega} e^{-\frac{\widetilde{\omega}^2}{2\Omega_d^2} + i\widetilde{\omega}\left[T_r + T_s - \tau_o(\vec{\boldsymbol{x}}_r, \vec{\boldsymbol{y}}^S) - \tau_o(\vec{\boldsymbol{x}}_s, \vec{\boldsymbol{y}}^S)\right]}.$$

Proposition 5.1 follows by integration over $\widetilde{\boldsymbol{x}}_r, \widetilde{\boldsymbol{x}}_s$ and $\widetilde{\omega}$. $\square$.

REFERENCES

[1] R.J. Adler, *The geometry of random fields*, Wiley, London, 1981.

[2] R. Alonso, L. Borcea, G. Papanicolaou, and C. Tsogka, *Detection and imaging in strongly backscattering randomly layered media*, Inverse Problems, 27 (2011), p. 025004(43pp.).

[3] H. Ammari, J. Garnier, H. Kang, W.K. Park, and K. Solna, *Imaging schemes for perfectly conducting cracks*, SIAM J. Appl. Math., 71 (2011), pp. 68–91.

[4] H. Ammari, J. Garnier, and K. Solna, *A statistical approach to target detection and localization in the presence of noise*, Waves in Random and Complex Media, (to appear).

[5] B. Biondi, *3D seismic imaging*, Society of Exploration Geophysics, Tulsa, 2006.

[6] N. Bleistein, J.K. Cohen, and J.W. Stockwell, *Mathematics of multidimensional seismic imaging, migration, and inversion*, Springer, New York, 2001.

[7] L. Borcea, J. Garnier, G. Papanicolaou, and C. Tsogka, *Coherent interferometric imaging, time gating, and beamforming*. submitted in 2010 to Inverse Problems.

[8] L. Borcea, G. Papanicolaou, and C. Tsogka, *Interferometric array imaging in clutter*, Inverse Problems, 21 (2005), pp. 1419–1460.

[9] ———, *Adaptive interferometric imaging in clutter and optimal illumination*, Inverse Problems, 22 (2006), pp. 1405–1436.

[10] ———, *Coherent interferometric imaging in clutter*, Geophysics, 71 (2006), pp. SI165–SI175.

[11] ———, *Asymptotics for the space-time Wigner transform with applications to imaging*, Stochastic Differential Equations: Theory and Applications. Volume in Honor of Professor Boris L Rozovskii, PH Baxendale and SV Lototsky editors., Interdisciplinary Mathematical Sciences, 2 (2007).

[12] ———, *Adaptive Time-Frequency Detection and Filtering for Imaging in Heavy Clutter*, SIAM Imaging Science, (to appear 2011).

[13] M. Born and E. Wolf, *Principles of optics: Electromagnetic theory of propagation, interference and diffraction of light*, Cambridge University Press, Cambridge, 7 ed., 1999.

[14] J.C. Curlander and R.N. McDonough, *Synthetic aperture radar: systems and signal processing*, Wiley, New York, 1991.

[15] L.J. Fradkin, *Limits of validity of geometrical optics in weakly irregular media*, J. Opt. Soc. Am. A, 6 (1989), pp. 1315–1319.

[16] J.W. Hardy, *Adaptive optics for astronomical telescopes*, Oxford University Press, USA, 1998.

[17] G. Matheron, *Principles of geostatistics*, Economic Geology, 58 (1963), pp. 1246–1266.

[18] B.D. Ripley, *Spatial statistics*, Wiley-Blackwell, Hoboken, 2004.

[19] S.M. Rytov, Y.A. Kravtsov, and V.I. Tatarskii, *Principles of statistical radiophysics. 4. Wave Propagation through random media*, Springer Verlag, Berlin, 1989.

[20] L. Ryzhik, G. Papanicolaou, and J.B. Keller, *Transport equations for elastic and other waves in random media*, Wave motion, 24 (1996), pp. 327–370.

[21] V.I. Tatarski, *Wave propagation in a turbulent medium*, Dover, New York, 1961.

[22] R. Tyson, *Principles of adaptive optics*, CRC Press, Boca Raton, 2010.

[23] B.S. White, *The stochastic caustic*, SIAM J. Appl. Math., 44 (1984), pp. 127–149.